

Entanglement spreading after local fermionic excitations in the XXZ chain

Matthias Gruber, Viktor Eisler

Institute of Theoretical and Computational Physics, Graz University of Technology,
NAWI Graz, Petersgasse 16, 8010 Graz, Austria

October 19, 2020

1 Abstract

2 We study the spreading of entanglement produced by the time evolution of a
3 local fermionic excitation created above the ground state of the XXZ chain.
4 The resulting entropy profiles are investigated via density-matrix renormaliza-
5 tion group calculations, and compared to a quasiparticle ansatz. In particular,
6 we assume that the entanglement is dominantly carried by spinon excitations
7 traveling at different velocities, and the entropy profile is reproduced by a
8 probabilistic expression involving the density fraction of the spinons reach-
9 ing the subsystem. The ansatz works well in the gapless phase for moderate
10 values of the XXZ anisotropy, eventually deteriorating as other types of quasi-
11 particle excitations gain spectral weight. Furthermore, if the initial state is
12 excited by a local Majorana fermion, we observe a nontrivial rescaling of the
13 entropy profiles. This effect is further investigated in a conformal field theory
14 framework, carrying out calculations for the Luttinger liquid theory. Finally,
15 we also consider excitations creating an antiferromagnetic domain wall in the
16 gapped phase of the chain, and find again a modified quasiparticle ansatz with
17 a multiplicative factor.

18

19 Contents

20	1 Introduction	2
21	2 XXZ chain and low-energy excitations	3
22	3 Entanglement dynamics in the gapless phase	6
23	3.1 Entanglement spreading in the quasiparticle picture	6
24	3.2 Local fermionic excitation	7
25	3.3 Local Majorana excitation	9
26	4 Entanglement after local excitations in CFT	10
27	4.1 Fermionic excitation	13
28	4.2 Majorana excitation	14
29	5 Entanglement dynamics in the gapped phase	16
30	5.1 Magnetization profiles	19
31	6 Summary and discussion	21
32	A Correlation functions of vertex operators	23

36

1 Introduction

37 The non-equilibrium dynamics of integrable models has developed into a vast field of
38 research [1]. Among the numerous aspects, the understanding of local relaxation and
39 equilibration in closed quantum systems has become a central topic of investigation [2, 3].
40 In this respect, integrable systems show a rather peculiar behaviour, as the dynamics
41 is characterized by the existence of stable quasiparticle excitations. This is intimately
42 related to the extensive number of nontrivial conservation laws, which nevertheless allow
43 for a local relaxation in a generalized sense [4].

44 Starting from the early studies of this topic, it was identified that the spreading of
45 entanglement must play a key role in our understanding of integrable dynamics. Ground
46 states of homogeneous, local Hamiltonians have a low amount of entanglement, typically
47 satisfying an area law [5]. However, considering the time evolution with respect to a differ-
48 ent Hamiltonian as in the context of a global quantum quench [6], the rapid *linear* growth
49 of entanglement was attributed to the ballistic propagation of entangled quasiparticle
50 pairs [7]. These quasiparticles transmit entanglement over large distances, contributing to
51 the buildup of an extensive entropy within any given subsystem, which signals the onset
52 of some local thermalization. Specifically, in one-dimensional integrable chains it has been
53 verified that the entanglement entropy accumulated in a subsystem actually plays the role
54 of the thermal entropy as described by the generalized Gibbs ensemble [8–10].

55 The global quench is the simplest representative of an initial state that has an extensive
56 amount of energy above the ground state of the Hamiltonian governing the dynamics, thus
57 acting as a reservoir of quasiparticle excitations. The interpretation, however, becomes
58 more complicated if the initial state lies in the low-energy regime. A particular example
59 is the local quench, where the final Hamiltonian is disturbed only locally with respect
60 to the initial one, such as joining two initially separated quantum chains. At criticality,
61 the entanglement spreading can be captured via conformal field theory (CFT) [11–13],
62 predicting a slow *logarithmic* growth of the entropy, which was indeed observed in free-
63 fermion chains [14]. However, despite signatures of the underlying quasiparticle dynamics,
64 such as a light-cone spreading with the maximal group velocity, it is unclear how the
65 individual quasiparticles contribute to the entropy.

66 Yet another situation that has been studied intensively within CFT is the so-called local
67 operator excitation [15–17]. Here the low-energy initial state is excited from the vacuum
68 of the CFT by the insertion of a local primary operator, while the Hamiltonian is left
69 untouched. The disturbance has then a linear propagation, increasing the entanglement
70 of a segment only while passing through it, with a *constant* excess entropy determined
71 by the quantum dimension of the local primary [15–17]. The calculations have been
72 extended in various directions, considering fermionic [18] or descendant fields [19, 20],
73 multiple excitations [21], as well as the effects of finite temperatures [22] or boundaries [23].

74 Despite this increased attention, there have been much less studies on entanglement
75 spreading after local excitations in integrable quantum chains. The CFT predictions have
76 been tested on the critical transverse Ising [24] and XX chains [25], for various local
77 operators that are lattice analogs of primary or descendant fields. On the other hand,
78 entanglement spreading has also been considered in the non-critical ordered phase of the

79 Ising [26] and XY chains [27,28], starting from a domain-wall initial state excited by a local
 80 Majorana operator. Remarkably, the emerging profile of the excess entropy was shown to
 81 be captured by a simple probabilistic quasiparticle ansatz [28]. Indeed, taking into account
 82 the dispersive spreading of quasiparticles, only a certain fraction of the initially localized
 83 excitation will cross the subsystem boundary located at a certain distance. Interpreting
 84 this quasiparticle fraction as the probability of finding the excitation within the subsystem,
 85 the excess entropy is simply given by a binary expression [28].

86 Here we aim to extend the quasiparticle description of entanglement spreading to local
 87 fermionic excitations in the XXZ chain. Being a Bethe ansatz integrable interacting
 88 model [29,30], its quasiparticle content is much more complex than in the free-fermion
 89 systems considered so far. Nevertheless, since our local excitations probe the low-energy
 90 physics, it seems reasonable that the dominant weight is carried by low-lying spinon ex-
 91 citations, which we shall assume to build our quasiparticle ansatz. Compared against
 92 the profiles of the excess entropy, as obtained from density-matrix renormalization group
 93 (DMRG) calculations [31–33], we observe a good agreement after a local fermion creation
 94 for moderate values of the interaction. For larger interactions in the gapless phase, one
 95 finds deviations that can be attributed to different types of quasiparticles with higher
 96 energy.

97 We also study the profiles after a local Majorana excitation, which seem to be given by
 98 a simple rescaling of the spinon ansatz. This result is supplemented by CFT calculations
 99 carried out for the Luttinger liquid theory, which describes the low-energy physics of the
 100 XXZ chain. We find that, due to the left-right mixing of the chiral bosonic modes, the
 101 asymptotic excess entropy is doubled for the Majorana excitation, although with a very
 102 slow convergence towards this value. Finally, in the gapped phase of the chain we study
 103 the excess entropy profile after a local Majorana operator that excites an antiferromagnetic
 104 domain wall. Here our numerical results suggest that the spinon ansatz is multiplied by a
 105 nontrivial factor, related to the ground-state entropy.

106 The rest of the manuscript is structured as follows. In section 2 we introduce the
 107 XXZ chain and discuss its low-lying excitations. Section 3 is devoted to the study of
 108 entanglement spreading after local excitations in the gapless phase: we first introduce a
 109 quasiparticle ansatz for the excess entanglement, followed by our numerical studies of a
 110 fermion creation as well as a Majorana excitation. Our results for the gapless regime are
 111 complemented by a calculation of the Rényi entropy within a CFT framework in section 4.
 112 Finally, in section 5 we consider entanglement and magnetization profiles after a domain-
 113 wall excitation in the gapped regime. Our closing remarks are given in section 6, followed
 114 by an appendix containing the details of the CFT calculations.

115 2 XXZ chain and low-energy excitations

116 We consider an XXZ chain of length L with open boundary conditions that is given by
 117 the Hamiltonian

$$H = J \sum_{j=-L/2+1}^{L/2-1} \left(S_j^x S_{j+1}^x + S_j^y S_{j+1}^y + \Delta S_j^z S_{j+1}^z \right), \quad (1)$$

118 where $S_j^\alpha = \sigma_j^\alpha/2$ are spin-1/2 operators acting on site j , and Δ is the anisotropy. The
 119 energy scale is set by the coupling J which we fix at $J = 1$. The XXZ Hamiltonian (1)
 120 conserves the total magnetization S^z in z -direction and we will be interested in its ground
 121 state in the zero-magnetization sector $S^z = 0$. Equivalently, the XXZ spin chain can be

122 rewritten in terms of spinless fermions by performing a Jordan-Wigner transformation,
 123 which brings (1) into the form

$$H = \sum_{j=-L/2+1}^{L/2-1} \left[\frac{1}{2}(c_j^\dagger c_{j+1} + c_{j+1}^\dagger c_j) + \Delta \left(c_j^\dagger c_j - \frac{1}{2} \right) \left(c_{j+1}^\dagger c_{j+1} - \frac{1}{2} \right) \right], \quad (2)$$

124 where c_j^\dagger (c_j) are fermionic creation (annihilation) operators, satisfying anticommutation
 125 relations $\{c_i, c_j^\dagger\} = \delta_{ij}$. One then has a half-filled fermionic hopping chain with nearest-
 126 neighbour interactions of strength Δ . For $|\Delta| \leq 1$ the system is in a critical phase with
 127 gapless excitations above the ground state, whereas a gap opens for $|\Delta| > 1$. The case
 128 $\Delta = 1$ corresponds to the isotropic Heisenberg antiferromagnet.

129 In the following we give a short and non-technical introduction to the construction
 130 of the ground state and low-lying excited states of the XXZ chain. To keep the discus-
 131 sion simple, we shall rather consider a periodic chain, and focus on the behaviour in the
 132 thermodynamic limit $L \rightarrow \infty$. The exact eigenstates of the XXZ chain can be found
 133 from Bethe ansatz [29, 30]. These are constructed as a superposition of plane waves, the
 134 so-called magnons, labeled by their rapidities λ_i which provide a convenient parametriza-
 135 tion of the quasimomenta. The allowed values of the rapidities follow from the Bethe
 136 equations, with real solutions corresponding to spin-wave like states. Complex solutions
 137 organize themselves into strings and correspond to bound states.

138 For $|\Delta| < 1$ the half-filled ground state is obtained by occupying all the allowed
 139 vacancies of the $L/2$ real rapidities, thus forming a tightly packed Fermi sea. Low-energy
 140 excitations in the $S^z = 1$ sector are called spinons and are created by removing a rapidity.
 141 This creates two holes in the Fermi sea, with all the remaining rapidities moving slightly
 142 with respect to their ground-state values, and the energy difference can be calculated from
 143 this back-flow effect. In the thermodynamic limit, the result can be found analytically and
 144 written directly in terms of the quasimomenta q_1 and q_2 of the two spinons as [29]

$$\Delta E = \varepsilon_s(q_1) + \varepsilon_s(q_2), \quad (3)$$

145 where the spinon dispersion relation in the gapless regime with $\Delta = \cos(\gamma)$ is given by

$$\varepsilon_s(q) = \frac{\pi \sin(\gamma)}{2} \frac{\sin(\gamma)}{\gamma} \sin(q). \quad (4)$$

146 Note that spinons are always excited in pairs, with the individual momenta confined to
 147 $0 \leq q_{1,2} \leq \pi$. The total momentum is then given by $q_1 + q_2$, and due to the additivity
 148 of (3) one actually has a band of excitation energies. In particular, the lower edge of the
 149 two-spinon band is obtained by setting $q_2 = 0$ or $q_2 = \pi$, and thus simply corresponds to
 150 shifting the dispersion in (4) for $q > \pi$. The group velocity of the spinons can be directly
 151 obtained from the derivative of the dispersion

$$v_s(q) = \frac{d\varepsilon_s(q)}{dq} = \frac{\pi \sin(\gamma)}{2} \frac{\sin(\gamma)}{\gamma} \cos(q). \quad (5)$$

152 Further low-energy excitations with $S^z = 1$ can be created by removing a single rapidity
 153 from the real axis and placing it onto the $\text{Im } \lambda = \pi$ axis. The energy of this particle-hole
 154 excitation can be obtained, similarly to the spinon case, from the back-flow equations of
 155 the rapidities and yields the dispersion [29]

$$\varepsilon_{ph}(q) = \pi \frac{\sin(\gamma)}{\gamma} \left| \sin\left(\frac{q}{2}\right) \right| \sqrt{1 + \cot^2\left(\frac{\pi}{2} \left(\frac{\pi}{\gamma} - 1\right)\right) \sin^2\left(\frac{q}{2}\right)}. \quad (6)$$

156 However, in contrast to spinons, particle-hole excitations are not composite objects and
 157 their momentum range is thus $0 \leq q < 2\pi$. Note that these spin-wave like excitations
 158 are only physical for $-1 < \Delta < 0$, i.e. in case of attractive interactions. For low mo-
 159 menta $q \rightarrow 0$, the dispersion relation Eq. (6) approaches the one for spinons in Eq. (4).
 160 The group velocities of particle-hole excitations are obtained by taking the derivative of
 161 $\varepsilon_{ph}(q)$. Interestingly, it was found that the maximum particle-hole velocity can exceed
 162 the maximum spinon velocity only if the anisotropy satisfies $\Delta < \Delta^* \approx -0.3$, which was
 163 demonstrated in a particular quench protocol [34].

164 Finally, we consider the gapped phase where we focus exclusively on the antiferromag-
 165 netic regime $\Delta > 1$, with the standard parametrization $\Delta = \cosh \phi$. For even L the ground
 166 state has $S^z = 0$ and is again given by $L/2$ magnons with real rapidities. However, the
 167 allowed number of vacancies is now $L/2 + 1$, which allows to construct a slightly shifted
 168 Fermi sea. In the Ising limit $\Delta \rightarrow \infty$, this yields an exact twofold degenerate ground state,
 169 given by the linear combinations of the two Néel states

$$|\psi_{\pm}\rangle = \frac{|\uparrow\downarrow\uparrow\downarrow\dots\rangle \pm |\downarrow\uparrow\downarrow\uparrow\dots\rangle}{\sqrt{2}}. \quad (7)$$

170 For finite Δ , the two states $|\psi_{\pm}\rangle$ constructed this way are only quasi-degenerate, with an
 171 energy difference decaying exponentially in the system size L . Considering the thermody-
 172 namic limit one can write

$$|\psi_{\pm}\rangle = \frac{|\psi_{\uparrow}\rangle \pm |\psi_{\downarrow}\rangle}{\sqrt{2}}, \quad (8)$$

173 where $|\psi_{\uparrow}\rangle$ and $|\psi_{\downarrow}\rangle$ correspond to ground states with spontaneously broken symmetry,
 174 displaying antiferromagnetic ordering. In fact, the bulk expectation value of the staggered
 175 magnetization can be calculated analytically as [35, 36]

$$\langle\psi_{\uparrow}|\sigma_j^z|\psi_{\uparrow}\rangle = -\langle\psi_{\downarrow}|\sigma_j^z|\psi_{\downarrow}\rangle = (-1)^j \prod_{n=1}^{\infty} \tanh^2(n\phi). \quad (9)$$

176 The low-lying excitations in the gapped phase are given again by spinons, by creating
 177 two holes in the Fermi sea. The excitation energy is still given by Eq. (3), with the
 178 dispersion in the gapped phase obtained as [29]

$$\varepsilon_s(q) = \frac{\sinh(\phi)}{\pi} K(u) \sqrt{1 - u^2 \cos^2(q)}, \quad (10)$$

179 where the complete elliptic integral of the first kind reads

$$K(u) = \int_0^{\pi/2} \frac{dp}{\sqrt{1 - u^2 \sin^2(p)}} \quad (11)$$

180 and the elliptic modulus u satisfies

$$\phi = \pi \frac{K(\sqrt{1 - u^2})}{K(u)}. \quad (12)$$

181 The spinon velocity is obtained from the derivative of (10) and reads

$$v_s(q) = \frac{\sinh(\phi)}{\pi} K(u) \frac{u^2 \sin(q) \cos(q)}{\sqrt{1 - u^2 \cos^2(q)}}. \quad (13)$$

182 3 Entanglement dynamics in the gapless phase

183 The goal of this section is to study the entanglement dynamics after a particular class of
 184 excitations. Namely, we first initialize the chain in its gapless ground state $|\psi_0\rangle$, which
 185 is then excited by an operator that is strictly local in terms of the creation/annihilation
 186 operators c_j^\dagger and c_j appearing in the fermionic representation (2) of the XXZ chain. The
 187 system is then let evolve freely and we are interested in the emerging entanglement pattern
 188 in the time-evolved state $|\psi(t)\rangle$. For a bipartition into a subsystem A and the rest of the
 189 chain B , this is characterized by the von Neumann entropy

$$S(t) = -\text{Tr}[\rho_A(t) \ln \rho_A(t)], \quad (14)$$

190 with the reduced density matrix $\rho_A(t) = \text{Tr}_B \rho(t)$ and $\rho(t) = |\psi(t)\rangle \langle \psi(t)|$. In particular,
 191 we consider the bipartition $A = [-L/2 + 1, r]$ and $B = [r + 1, L/2]$ and study the entropy
 192 profiles

$$\Delta S = S(t) - S(0) \quad (15)$$

193 along the chain by varying r , where $r = 0$ corresponds to the half-chain. Note that by
 194 subtracting the ground-state entropy $S(0)$, we aim to extract information about the excess
 195 entanglement created by a local excitation.

196 In the following subsections we first introduce an intuitive picture for the description of
 197 the entanglement spreading in terms of the low-lying quasiparticle excitations introduced
 198 in Sec. 2. We then proceed to the numerical study of the entanglement profiles after
 199 exciting the ground state with a fermionic creation operator, and compare the results to
 200 our quasiparticle ansatz. In the last part we consider an excitation created by a local
 201 Majorana fermion operator.

202 3.1 Entanglement spreading in the quasiparticle picture

203 Let us consider an excitation above the ground state of the XXZ chain by acting with a
 204 fermion creation operator c_j^\dagger . To capture the dynamics, one would have to first decompose
 205 the initial local excited state in the eigenbasis of the Hamiltonian. As discussed in the
 206 previous section, these eigenstates are described by quasiparticles parametrized by their
 207 rapidities or quasimomenta. The entanglement properties of various eigenstates in the
 208 XXZ chain were studied before in [37, 38], whereas a systematic CFT treatment of low-
 209 energy excitations was introduced in [39, 40]. In the framework of free quantum field
 210 theory, a surprisingly simple result on quasiparticle excitations was recently found in
 211 [41, 42]. Namely, the excess entanglement measured from the ground state was found to
 212 be completely independent of the quasiparticle momenta, depending only on the ratio p
 213 of the subsystem and full chain lengths. Moreover, for quasiparticles described by a single
 214 momentum, the excess entropy is given by a binary formula $\Delta S = -p \ln p - (1-p) \ln(1-p)$,
 215 which allows for a simple probabilistic interpretation. Indeed, the ratio p is just the
 216 probability of finding the quasiparticle within the subsystem.

217 Motivated by these results, we now put forward a simple ansatz for the spreading of
 218 entanglement after the local excitation. Under time evolution, the quasiparticles involved
 219 in the decomposition of the initial state spread out with their corresponding group ve-
 220 locities. However, our main assumption is that their contribution to entanglement is still
 221 independent of the momentum. Furthermore, we shall also assume that the dominant
 222 part of the entanglement is carried by the lowest-lying spinon modes, and that a spatially
 223 localized excitation translates to a homogeneous distribution of the momenta in the initial
 224 state. Under these assumptions we expect that the entanglement profile at time $t \gg 1$

225 and distance $r \gg 1$ from the excitation, in the space-time scaling limit $\zeta = r/t$ fixed, is
 226 determined exclusively via

$$\mathcal{N} = \int_0^\pi \frac{dq}{\pi} \Theta(v_s(q) - \zeta), \quad (16)$$

227 where $\Theta(x)$ is the Heaviside step function and $v_s(q)$ is the spinon velocity. In fact, this is
 228 nothing else but the fraction of the spinon modes with sufficient velocity to arrive at the
 229 subsystem. The simple probabilistic interpretation of the entanglement then leads to the
 230 binary entropy formula for the profile

$$\Delta S = -\mathcal{N} \ln(\mathcal{N}) - (1 - \mathcal{N}) \ln(1 - \mathcal{N}). \quad (17)$$

231 In particular, for the gapless case considered here, inserting the expression (5) of the spinon
 232 velocity into (16), the spinon fraction can immediately be found as

$$\mathcal{N} = \frac{1}{\pi} \arccos\left(\frac{\zeta}{v}\right), \quad (18)$$

233 where $v = v_s(0)$ denotes the maximal spinon velocity.

234 In summary, our simplistic ansatz (17) provides an interpretation of the excess entropy
 235 based on the dispersive dynamics of the quasiparticle modes, where \mathcal{N} is the fraction of
 236 the initially localized excitation that arrives at the subsystem. In fact, the very same
 237 ansatz has recently been suggested for the description of entanglement spreading after local
 238 fermionic excitations in the XY chain, finding an excellent agreement with numerics [28].
 239 Note, however, that the XY chain is equivalent to a free-fermion model and thus all
 240 the single-particle modes can exactly be included in \mathcal{N} . In contrast, for the interacting
 241 XXZ chain, restricting ourselves to the spinon modes should necessarily introduce some
 242 limitations to the quasiparticle ansatz, as demonstrated in the following subsection.

243 3.2 Local fermionic excitation

244 We continue with the numerical study of the excitation produced by the fermionic creation
 245 operator c_j^\dagger . The fermion operators are related to the spin variables via the Jordan-Wigner
 246 transformation

$$c_j^\dagger = \left(\prod_{l=-L/2+1}^{j-1} \sigma_l^z \right) \sigma_j^+, \quad c_j = \left(\prod_{l=-L/2+1}^{j-1} \sigma_l^z \right) \sigma_j^-, \quad (19)$$

247 where σ_j^α are the Pauli matrices and $\sigma_j^\pm = (\sigma_j^x \pm i\sigma_j^y)/2$. For simplicity, we shall only
 248 consider the case where the excitation is created by c_1^\dagger in the middle of the chain. The
 249 time-evolved state after the excitation is then given by

$$|\psi(t)\rangle = N^{-1/2} e^{-iHt} c_1^\dagger |\psi_0\rangle, \quad (20)$$

250 where $|\psi_0\rangle$ is the ground state and the normalization is given by

$$N = \langle \psi_0 | c_1 c_1^\dagger | \psi_0 \rangle = 1/2 \quad (21)$$

251 as the ground state is half filled. The time evolution is actually implemented via time-
 252 dependent DMRG (tDMRG) [43,44] in the spin-representation of the XXZ chain, by first
 253 carrying out the ground-state search and applying the string operator (19) onto the MPS
 254 representation of $|\psi_0\rangle$. The calculations were performed using the ITensor C++ library [45]

255 and a truncated weight of 10^{-9} .

256

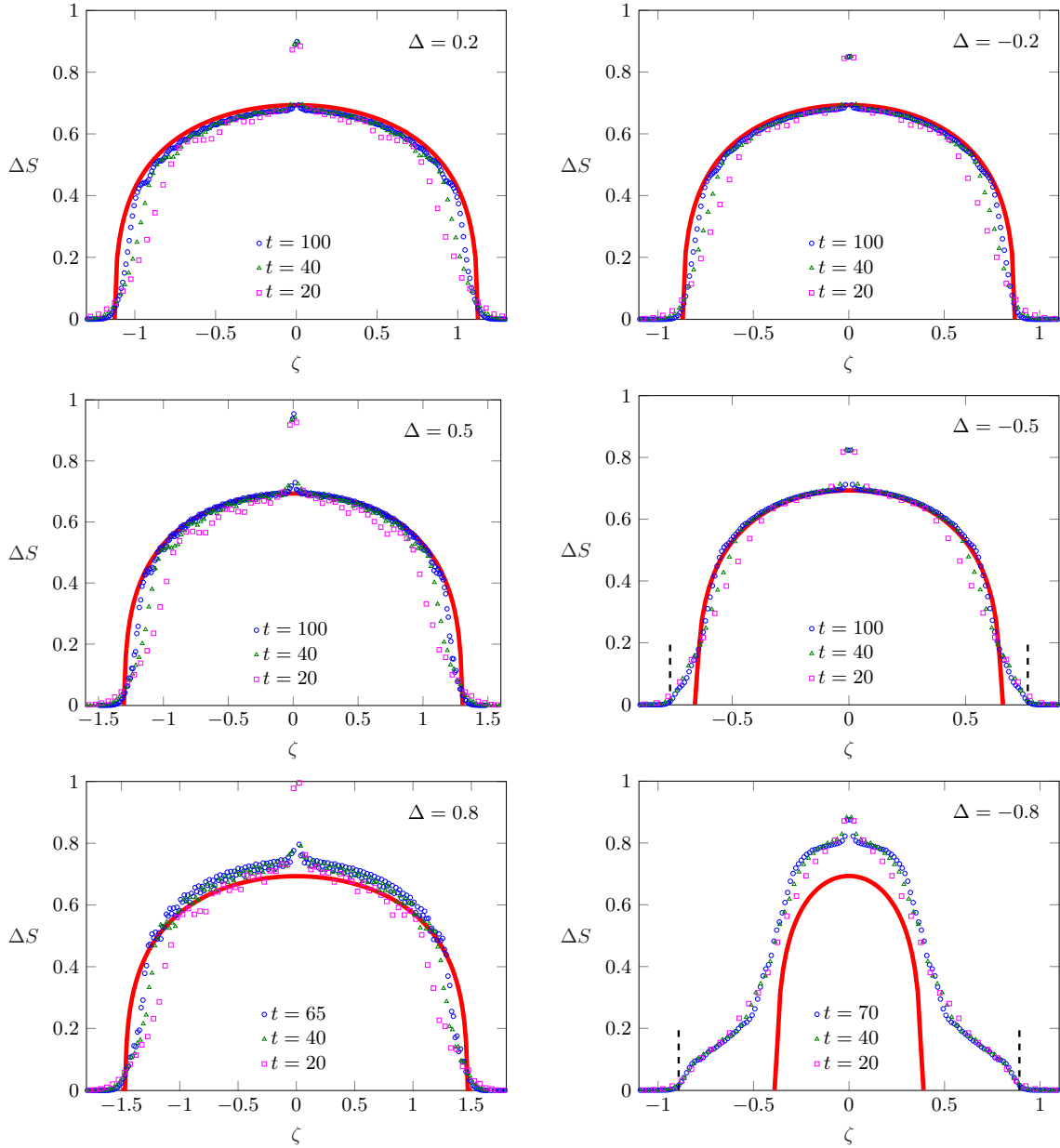


Figure 1: Excess entropy profiles ΔS obtained from tDMRG simulations at different times (symbols), after the excitation c_1^\dagger in a chain of length $L = 300$. The scaled profiles are plotted against $\zeta = r/t$ and compared to the quasiparticle ansatz (red lines) in Eq. (17). The dashed black lines denote the maximum velocity of the particle-hole excitations, derived from Eq. (6).

257 The results of our simulations are shown in Fig. 1 for various interaction strengths
 258 Δ . The different symbols correspond to snapshots of the entropy profile ΔS at different
 259 times, plotted against the scaled distance $\zeta = r/t$. The quasiparticle ansatz (17) computed
 260 using the spinon fraction (18) is shown by the red solid lines. For moderate values of $|\Delta|$,
 261 one observes a very good agreement with the numerical profiles, except for a peak around
 262 $\zeta = 0$. Note that this peak rises above the maximum value $\ln(2)$ that can be obtained

263 from the spinon ansatz. A closer inspection for $r = 0$ indicates that the entropy peak also
 264 converges to a finite value for large times, with a nontrivial dependence on Δ . Moreover,
 265 one can also observe a slight broadening of the peak for larger Δ . However, the precise
 266 origin of the peak cannot be understood within our simple quasiparticle ansatz.

267 Systematic deviations from (17) also occur for larger Δ , especially in the attractive
 268 regime. Indeed, for $\Delta = -0.5$ one already observes that the edges of the profile obtained
 269 from numerics fall slightly outside of the spinon edge, whereas the bulk profile still shows
 270 a good agreement. For $\Delta = -0.8$ the mismatch becomes more drastic both in the bulk
 271 and around the edges, signaling the breakdown of the naive spinon ansatz. Clearly, for
 272 strong attractive interactions the local excited state should have significant overlaps with
 273 other quasiparticle excitations of the XXZ chain. In fact, as discussed in Sec. 2, in this
 274 regime the maximum velocity of particle-hole excitations exceeds the spinon velocity and
 275 matches perfectly the edges of the profile, as indicated by the black dashed lines in Fig. 1.
 276 Hence, the entropy spreading should be determined by the coexistence of the spinon and
 277 particle-hole excitations, allowing to reach values beyond $\ln(2)$. Presumably, improving
 278 the ansatz (17) would require the knowledge of the overlaps with the different families
 279 of quasiparticles. Finally, it should be noted that, even though the edge locations of the
 280 profile seem to be captured, significant deviations in the bulk also occur for large repulsive
 281 interactions (see $\Delta = 0.8$ in Fig. 1), which might be due to bound-state contributions.

282 3.3 Local Majorana excitation

283 As a second example, we are going to consider local Majorana excitations, given in terms
 284 of the spin variables via

$$m_{2j-1} = \left(\prod_{l=-L/2+1}^{j-1} \sigma_l^z \right) \sigma_j^x, \quad m_{2j} = \left(\prod_{l=-L/2+1}^{j-1} \sigma_l^z \right) \sigma_j^y, \quad (22)$$

285 and satisfying the anticommutation relations $\{m_k, m_l\} = 2\delta_{kl}$. Majorana operators are
 286 Hermitian and related to the fermion creation/annihilation operators as $m_{2j-1} = c_j + c_j^\dagger$
 287 and $m_{2j} = i(c_j - c_j^\dagger)$. Focusing again on an excitation m_1 in the middle of the chain, the
 288 time-evolved stated is now given by

$$|\psi(t)\rangle = e^{-iHt} m_1 |\psi_0\rangle. \quad (23)$$

289 The entanglement profiles ΔS obtained from tDMRG simulations of (23) are depicted
 290 in Fig. 2 for four different values of Δ . To visualize the spreading of the profile, we now plot
 291 the unscaled data against the location of the subsystem boundary. For $\Delta = 0$, the profile
 292 looks similar to that of the corresponding c_1^\dagger excitation and is indeed perfectly reproduced
 293 by the quasiparticle ansatz (17). However, in the interacting case $\Delta \neq 0$, one observes
 294 a marked difference when compared to the corresponding panels in Fig. 1. Namely, the
 295 profiles in Fig. 2 clearly exceed the value $\ln(2)$, indicated by the dashed horizontal lines,
 296 which is the maximum of the ansatz (17). Nevertheless, we observe that the profiles after
 297 the m_1^\dagger excitations can be well described by a simple rescaling of the spinon ansatz (17),
 298 as shown by the solid lines in Fig. 2. The constant factor multiplying the ansatz is chosen
 299 such that the maxima of the profiles at $r = 0$ are correctly reproduced. Note also that the
 300 central peak observed for the c_1^\dagger excitation in Fig. 1 is missing for the Majorana excitation.

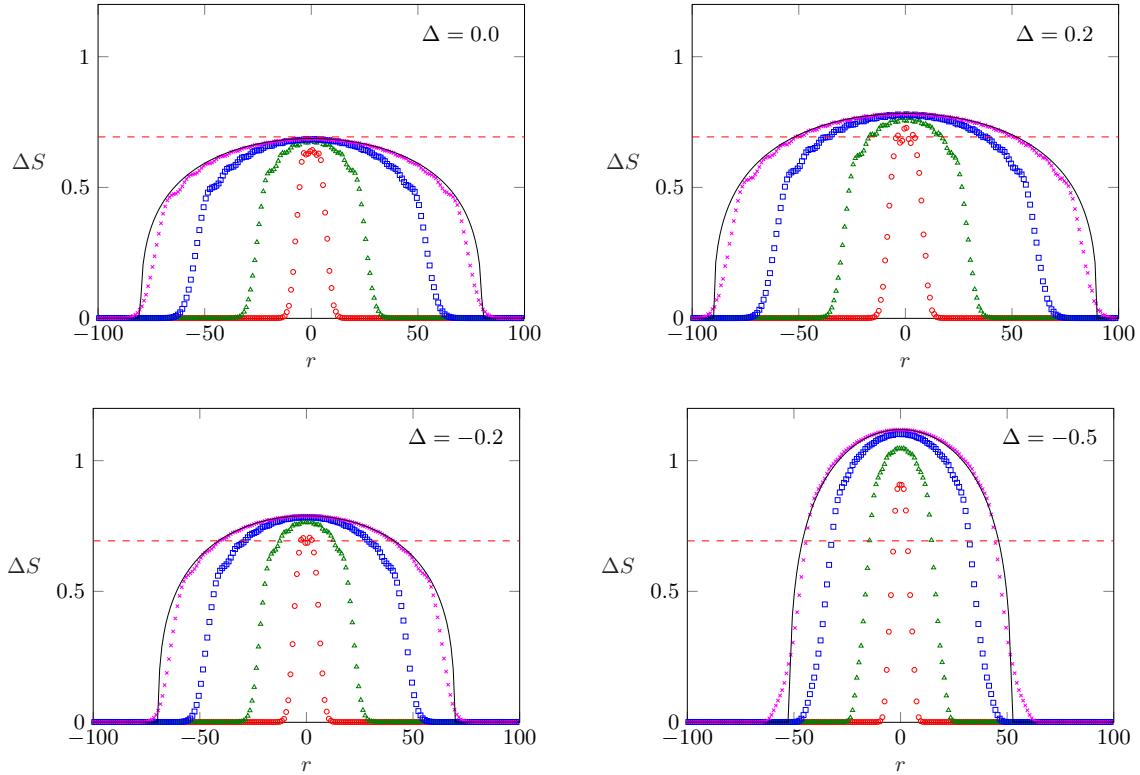


Figure 2: Excess entropy profiles ΔS as a function of r at times $t = 10, 30, 60, 80$ (red, green, blue, magenta) after the Majorana excitation m_1 for four different values of Δ and $L = 200$. The red dashed lines indicate the value $\ln(2)$. The black solid lines show the spinon ansatz Eq. (17) for $t = 80$, multiplied by a constant to match the maxima of the profiles.

301 To better understand the behaviour of the maxima, on the left of Fig. 3 we plot the
 302 time evolution of the excess entropy ΔS in the middle of the chain ($r = 0$) with $L = 200$
 303 and for various Δ . One observes that the asymptotic value of the excess entropy grows
 304 with increasing $|\Delta|$, approaching its maximum very slowly in time. In fact, for even larger
 305 times the entropy starts to decrease again as one approaches $vt \approx L$, when the fastest
 306 spinons leave the subsystem after a reflection from the chain end. This is demonstrated
 307 on the right of Fig. 3 by repeating the calculations for a smaller chain with $L = 50$. The
 308 emergence of a plateau is clearly visible, which then immediately repeats itself for $vt > L$
 309 due to the symmetry of the geometry, with the spinons reflected from the other end of the
 310 chain entering the subsystem again. However, the question why the height of the plateau
 311 depends on the interaction strength Δ can only be answered via a more involved CFT
 312 analysis of the problem, which is presented in the next section.

313 4 Entanglement after local excitations in CFT

314 The low-energy physics of the gapless XXZ chain can be captured within quantum field
 315 theory via the bosonization procedure [46]. Using the fermionic representation (2) of the
 316 chain, one introduces the Heisenberg operators $c(x, \tau) = e^{\tau H} c_x e^{-\tau H}$, where x is the spatial
 317 coordinate along the chain and we introduced the imaginary time $\tau = it$. Linearizing the
 318 dispersion around the Fermi points, one can approximate

$$c(x, \tau) \simeq e^{ik_F x} \psi(x, \tau) + e^{-ik_F x} \bar{\psi}(x, \tau), \quad (24)$$

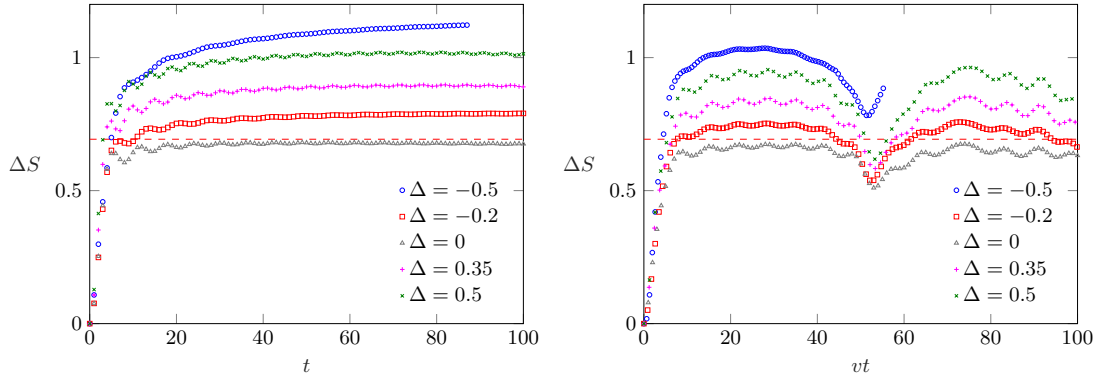


Figure 3: Left: Entropy growth in the middle of the chain $r = 0$, after the Majorana excitation m_1 for different values of Δ and $L = 200$. The red dashed line indicates the value $\ln(2)$. Right: ΔS for a smaller chain with $L = 50$ against the scaled time vt for the same Δ values.

319 where $\psi(x, \tau)$ and $\bar{\psi}(x, \tau)$ are the right and left-moving components of a fermion field.
 320 The phase factors with the Fermi momentum, where $k_F = \pi/2$ for a half-filled chain,
 321 are included to ensure that the chiral fermions are described by slowly varying fields.
 322 Introducing the complex coordinates $w = v\tau - ix$ and $\bar{w} = v\tau + ix$, where v denotes the
 323 Fermi velocity, they can be written in a bosonized form [46]

$$\psi(w) = \frac{1}{\sqrt{2\pi}} e^{-i\sqrt{4\pi}\varphi(w)}, \quad \bar{\psi}(\bar{w}) = \frac{1}{\sqrt{2\pi}} e^{i\sqrt{4\pi}\bar{\varphi}(\bar{w})}, \quad (25)$$

324 where $\varphi(w)$ and $\bar{\varphi}(\bar{w})$ are the chiral boson fields. In terms of the new bosonic variables

$$\phi = \varphi + \bar{\varphi}, \quad \theta = \varphi - \bar{\varphi}, \quad (26)$$

325 one can show that the bosonized form of the XXZ chain (2) is described by the Luttinger
 326 liquid Hamiltonian [47]

$$H_{LL} = \frac{v}{2} \int dx [K(\partial_x \theta)^2 + K^{-1}(\partial_x \phi)^2]. \quad (27)$$

327 Apart from the velocity v , the Hamiltonian (27) is characterized by the Luttinger param-
 328 eter K . Both of them can be fixed from the exact Bethe ansatz solution as

$$v = \frac{\pi \sin(\gamma)}{2\gamma}, \quad K = \frac{1}{2} \left(1 - \frac{\gamma}{\pi}\right)^{-1}, \quad (28)$$

329 with the usual parametrization $\Delta = \cos(\gamma)$. Note that $v = v_s(0)$ is just the maximum of
 330 the spinon velocity (5).

331 In CFT language, the Luttinger liquid corresponds to a free compact boson field theory.
 332 In order to study entanglement evolution after local operator excitations, we shall thus
 333 use the framework developed for a generic CFT [15, 16]. In the following we summarize
 334 the main steps of the procedure. Let us consider the state

$$|\psi\rangle = N^{-1/2} \mathcal{O}(-d) |0\rangle \quad (29)$$

335 excited from the CFT vacuum $|0\rangle$ by insertion of the local operator $\mathcal{O}(-d)$, where N
 336 accounts for the normalization of the state. For the sake of generality, we consider the

337 situation where the excitation is inserted at a distance d measured from the center of the
338 chain. After time evolution, the density matrix reads

$$\rho(t) = N^{-1} e^{-iHt} e^{-\epsilon H} \mathcal{O}(-d) |0\rangle \langle 0| \mathcal{O}^\dagger(-d) e^{-\epsilon H} e^{iHt}, \quad (30)$$

339 where ϵ is a UV regularization that is required for the state to be normalizable. Working
340 in a Heisenberg picture, the time evolution can be absorbed into the operators, and the
341 state can be represented as

$$\rho(t) = \frac{\mathcal{O}(w_2, \bar{w}_2) |0\rangle \langle 0| \mathcal{O}^\dagger(w_1, \bar{w}_1)}{\langle \mathcal{O}^\dagger(w_1, \bar{w}_1) \mathcal{O}(w_2, \bar{w}_2) \rangle}, \quad (31)$$

342 where the complex coordinates of the operator insertions are given by

$$\begin{aligned} w_1 &= -i(vt - d) + \epsilon, & \bar{w}_1 &= -i(vt + d) + \epsilon, \\ w_2 &= -i(vt - d) - \epsilon, & \bar{w}_2 &= -i(vt + d) - \epsilon. \end{aligned} \quad (32)$$

343 It should be stressed that the \bar{w}_j coordinates are actually not the complex conjugates of
344 w_j , as we are assuming $\tau = it$ to be real, such that we can work with Euclidean spacetime.

345 With the expression (31) at hand, one can proceed to construct the path-integral
346 representation of the reduced density matrix, by opening a cut at $\tau = 0$ along the spatial
347 coordinates of the subsystem A . The Rényi entropy

$$S_n(t) = \frac{1}{1-n} \ln \text{Tr} [\rho_A^n(t)] \quad (33)$$

348 for integer n can then be obtained by applying the replica trick [48], i.e. sewing together
349 n copies of the path integrals cyclically along the cuts. In turn, one can express the
350 excess Rényi entropy $\Delta S_n = S_n(t) - S_n(0)$ via correlation functions of the local operator
351 as [15, 16]

$$\Delta S_n = \frac{1}{1-n} \log \left[\frac{\langle \mathcal{O}^\dagger(w_1, \bar{w}_1) \mathcal{O}(w_2, \bar{w}_2) \dots \mathcal{O}(w_{2n}, \bar{w}_{2n}) \rangle_{\Sigma_n}}{\langle \mathcal{O}^\dagger(w_1, \bar{w}_1) \mathcal{O}(w_2, \bar{w}_2) \rangle_{\Sigma_1}^n} \right], \quad (34)$$

352 where Σ_n denotes the n -sheeted Riemann surface, with w_1, \dots, w_{2n} and $\bar{w}_1, \dots, \bar{w}_{2n}$ being
353 the replica coordinates of the insertion points (32).

354 Although the expression (34) for the excess Rényi entropy is very general, the calcu-
355 lation of $2n$ -point functions on the complicated Riemann surface Σ_n may become rather
356 involved. However, if the subsystem A is given by a single interval $0 \leq x \leq \ell$ in an infinite
357 chain, the geometry can be simplified by the conformal transformation

$$z = \left(\frac{w}{w + i\ell} \right)^{1/n}, \quad \bar{z} = \left(\frac{\bar{w}}{\bar{w} - i\ell} \right)^{1/n}, \quad (35)$$

358 which maps the n -sheeted surface onto a single Riemann sheet. This transformation leads
359 to the holomorphic coordinates of the operator insertions

$$z_{2j-1} = e^{2\pi i j/n} \left(\frac{d - vt - i\epsilon}{\ell + d - vt - i\epsilon} \right)^{1/n}, \quad z_{2j} = e^{2\pi i j/n} \left(\frac{d - vt + i\epsilon}{\ell + d - vt + i\epsilon} \right)^{1/n}, \quad (36)$$

360 while the anti-holomorphic ones are given by

$$\bar{z}_{2j-1} = e^{-2\pi i j/n} \left(\frac{d + vt + i\epsilon}{\ell + d + vt + i\epsilon} \right)^{1/n}, \quad \bar{z}_{2j} = e^{-2\pi i j/n} \left(\frac{d + vt - i\epsilon}{\ell + d + vt - i\epsilon} \right)^{1/n}. \quad (37)$$

361 Furthermore, if the local operators are primary fields of the CFT with respective conformal
362 dimensions $h_{\mathcal{O}}$ and $\bar{h}_{\mathcal{O}}$, the $2n$ -point function transforms as

$$\langle \prod_{j=1}^n \mathcal{O}^\dagger(w_{2j-1}, \bar{w}_{2j-1}) \mathcal{O}(w_{2j}, \bar{w}_{2j}) \rangle_{\Sigma_n} = \prod_{i=1}^{2n} \left(\frac{dw}{dz} \right)_{z_i}^{-h_{\mathcal{O}}} \left(\frac{d\bar{w}}{d\bar{z}} \right)_{\bar{z}_i}^{-\bar{h}_{\mathcal{O}}} \langle \prod_{j=1}^n \mathcal{O}^\dagger(z_{2j-1}, \bar{z}_{2j-1}) \mathcal{O}(z_{2j}, \bar{z}_{2j}) \rangle_{\Sigma_1}. \quad (38)$$

363 In the end, one is left with a problem of calculating $2n$ -point functions on the complex
364 plane. For the sake of simplicity, in the following we shall only consider the case $n = 2$,
365 and apply the procedure outlined above to the Luttinger liquid theory, with the local
366 excitations considered in section 3.

367 4.1 Fermionic excitation

368 We start with the fermion creation operator, which after bosonization (25) corresponds to
369 the field insertion

$$\mathcal{O}_f(w, \bar{w}) = e^{ik_F d} e^{i\sqrt{4\pi}\varphi(w)} + e^{-ik_F d} e^{-i\sqrt{4\pi}\bar{\varphi}(\bar{w})}, \quad (39)$$

370 where we omitted normalization factors that cancel in the expression (34). Clearly,
371 $\mathcal{O}_f(w, \bar{w})$ is not itself a primary operator but rather a linear combination of two. Hence,
372 the calculation of the four-point function that appears in ΔS_2 involves a number of terms
373 with primaries, each of which can be mapped from Σ_2 to the complex plane using the
374 transformation rule (38). The calculation of these correlation functions can be facilitated
375 by first performing a canonical transformation

$$\theta' = \sqrt{K}\theta, \quad \phi' = \frac{1}{\sqrt{K}}\phi. \quad (40)$$

376 which absorbs the Luttinger parameter K in the Hamiltonian (27). However, since the
377 variables θ and ϕ are actually linear combinations (26) of the chiral bosons, the change of
378 variables corresponds to the Bogoliubov transformation

$$\varphi = \cosh(\xi)\varphi' + \sinh(\xi)\bar{\varphi}' \quad \bar{\varphi} = \sinh(\xi)\varphi' + \cosh(\xi)\bar{\varphi}', \quad (41)$$

379 where $K = e^{2\xi}$. Thus, the transformation of the Luttinger liquid Hamiltonian induces a
380 left-right mixing of the chiral bosonic modes. In the following we shall use the shorthand
381 notations $c = \cosh(\xi)$ and $s = \sinh(\xi)$.

382 Clearly, our task now boils down to evaluate correlation functions of vertex operators

$$V_{\alpha,\beta}(z, \bar{z}) = e^{i\sqrt{4\pi}\alpha\varphi'(z) + i\sqrt{4\pi}\beta\bar{\varphi}'(\bar{z})} \quad (42)$$

383 on the complex plane with respect to the Luttinger liquid theory scaled to the free-fermion
384 point. The n -point function of vertex operators is then well known and given by [49]

$$\langle \prod_{j=1}^n V_{\alpha_i, \beta_i}(z_i, \bar{z}_i) \rangle = \prod_{i < j} (z_i - z_j)^{\alpha_i \alpha_j} (\bar{z}_i - \bar{z}_j)^{\beta_i \beta_j}, \quad (43)$$

385 where the neutrality conditions

$$\sum_{i=1}^n \alpha_i = 0, \quad \sum_{i=1}^n \beta_i = 0 \quad (44)$$

386 must be satisfied, otherwise the correlator vanishes. In particular, considering the two-
387 point function one immediately sees that the vertex operator (42) is a primary with scaling
388 dimensions $h = \alpha^2/2$ and $\bar{h} = \beta^2/2$.

389 With all the ingredients at hand, performing the calculation for ΔS_2 is a straightfor-
 390 ward but cumbersome exercise, and we refer to Appendix A for the main details. It turns
 391 out that the result depends only on the cross-ratios

$$\eta = \frac{z_{12}z_{34}}{z_{13}z_{24}}, \quad \bar{\eta} = \frac{\bar{z}_{12}\bar{z}_{34}}{\bar{z}_{13}\bar{z}_{24}} \quad (45)$$

392 of the holomorphic and anti-holomorphic coordinates (36) and (37), where $z_{ij} = z_i - z_j$ and
 393 $\bar{z}_{ij} = \bar{z}_i - \bar{z}_j$, respectively. In terms of the cross-ratios, the final result reads

$$\Delta S_2 = -\ln \left(\frac{1 + |\eta|^{(c+s)^2} + |1 - \eta|^{(c+s)^2}}{2} \right). \quad (46)$$

394 It is important to stress that the notation $|\eta|$ should be understood as $(\eta\bar{\eta})^{1/2}$, since the
 395 two cross ratios are not conjugate variables. In particular, in the limit $\epsilon \rightarrow 0$ of the
 396 regularization, one has the behaviour [15, 16]

$$\lim_{\epsilon \rightarrow 0} \eta = \begin{cases} 0 & \text{if } 0 < vt < d \text{ or } vt > d + \ell \\ 1 & \text{if } d < vt < d + \ell \end{cases}, \quad \lim_{\epsilon \rightarrow 0} \bar{\eta} = 0. \quad (47)$$

397 This yields the following limit for the Rényi entropy

$$\lim_{\epsilon \rightarrow 0} \Delta S_2 = \begin{cases} 0 & \text{if } 0 < vt < d \text{ and } vt > d + \ell \\ \ln(2) & \text{if } d < vt < d + \ell \end{cases}. \quad (48)$$

398 The result has a very simple interpretation. Namely, our excitation is an equal super-
 399 position of a left- and right-moving fermion, and the entanglement is changed by $\ln(2)$ only
 400 when the right-moving excitation is located within the interval. In fact, this is exactly
 401 the same picture that lies behind the quasiparticle ansatz (17), without the dispersion
 402 of the wavefront. Interestingly, apart from the presence of the spinon velocity v , the
 403 limiting result (48) is independent of the anisotropy Δ . The only effect of the left-right
 404 boson mixing appears in the exponents of the cross-ratios in (46), which simply determines
 405 how the sharp step-function for ΔS_2 is rounded off for finite UV regularizations. In fact,
 406 this result is very similar to the one obtained for a non-chiral EPR-primary excitation in
 407 Ref. [16, 19]. Moreover, this is also a simple generalization of the result in Ref. [25], where
 408 the superposition of purely holomorphic and anti-holomorphic primaries was considered.

409 4.2 Majorana excitation

410 We move on to consider the Majorana excitation

$$\mathcal{O}_m(w, \bar{w}) = \mathcal{O}_f(w, \bar{w}) + \mathcal{O}_f^\dagger(w, \bar{w}). \quad (49)$$

411 The calculation of ΔS_2 follows the exact same procedure as for $\mathcal{O}_f(w, \bar{w})$, however, one
 412 has now an even larger number of terms to consider. The main steps are again outlined
 413 in Appendix A, which lead to the result

$$\Delta S_2 = -\ln \left(\frac{2A + B + C}{8} \right), \quad (50)$$

414 where the terms in the logarithm are given by

$$A = |1 - \eta|^{(c+s)^2} + |1 - \eta|^{(c-s)^2} + |\eta|^{(c+s)^2} + |\eta|^{(c-s)^2} \quad (51)$$

$$B = 2 + \eta^{2c^2} \bar{\eta}^{2s^2} + \eta^{2s^2} \bar{\eta}^{2c^2} + (1 - \eta)^{2c^2} (1 - \bar{\eta})^{2s^2} + (1 - \eta)^{2s^2} (1 - \bar{\eta})^{2c^2} \quad (52)$$

$$C = \left[|\eta|^{(c+s)^2} |1 - \eta|^{(c-s)^2} + |\eta|^{(c-s)^2} |1 - \eta|^{(c+s)^2} \right] (Z + \bar{Z}) \quad (53)$$

415 and a new variable is introduced as

$$Z = \frac{z_1 \bar{z}_2 (1 - \bar{z}_1^2) (1 - z_2^2)}{\bar{z}_1 z_2 (1 - z_1^2) (1 - \bar{z}_2^2)}. \quad (54)$$

416 The result is thus rather involved and cannot be written as a function of the cross-
 417 ratios alone. However, in the limit $\epsilon \rightarrow 0$, the factors in A , B , and C can trivially be
 418 evaluated using (47), as well as using $Z \rightarrow 1$ and $\bar{Z} \rightarrow 1$. For the case $\Delta \neq 0$, this leads
 419 to the following simple result

$$\lim_{\epsilon \rightarrow 0} \Delta S_2 = \begin{cases} 0 & \text{if } 0 < vt < d \text{ and } vt > d + \ell \\ 2 \ln(2) & \text{if } d < vt < d + \ell \end{cases}. \quad (55)$$

420 In sharp contrast, for $\Delta = 0$, where $c = 1$ and $s = 0$, one recovers the result (48). Hence,
 421 one arrives at the rather surprising result that the excess entropy is doubled in case of
 422 interactions, which must be a consequence of the left-right boson mixing.

423 Obviously, for finite values of the regularization ϵ , this transition should take place
 424 continuously, rather than giving an abrupt jump. The behaviour of ΔS_2 for $\epsilon = 0.1$ is
 425 shown in Fig. 4 for an interval of length $\ell = 20$ at a distance $d = 10$ from the excitation.
 426 One can clearly see the development of a plateau for times $d < vt < d + \ell$, the height of
 427 which increases monotonously with Δ . Nevertheless, even for the largest value $\Delta = 0.8$,
 428 the expected maximum of $2 \ln(2)$ is by far not reached. The very slow convergence towards
 429 the $\epsilon \rightarrow 0$ (or, equivalently, $t \rightarrow \infty$) limit can be understood by looking at the structure
 430 of the terms appearing in (50). In fact, for smaller values of $|\Delta|$, the slowest converging
 431 pieces are given by $\eta^{2c^2} \bar{\eta}^{2s^2}$ as well as $(1 - \eta)^{2s^2} (1 - \bar{\eta})^{2c^2}$ in the expression (52) of B ,
 432 due to the large-time behaviour $\bar{\eta} \approx 1 - \eta \approx (\epsilon/2vt)^2$ for $d \ll vt \ll \ell + d$. Hence, the
 433 apparent nontrivial values of the plateau in Fig. 4 is a consequence of the very slow decay
 434 $(\epsilon/vt)^{4s^2}$, where the exponent for e.g. $\Delta = 0.5$ is given by $4s^2 \approx 0.08$. Clearly, observing
 435 convergence towards $\Delta S_2 \rightarrow 2 \ln(2)$ would require enormous time scales as well as interval
 436 lengths.

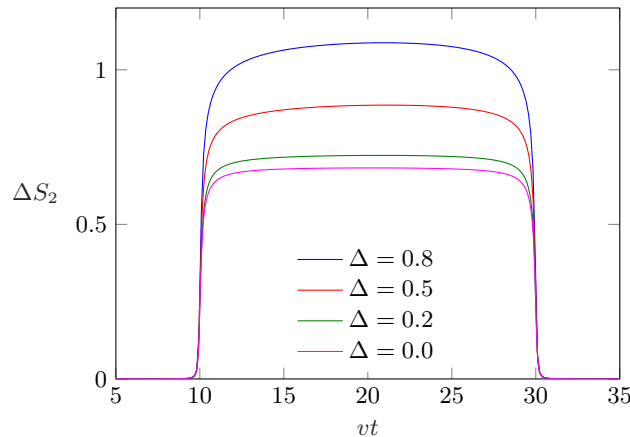


Figure 4: Time evolution of the excess Rényi entropy in Eq. (50) after the Majorana excitation with $\ell = 20$, $d = 10$ and $\epsilon = 0.1$.

437 Despite the different geometry considered for the CFT calculations, we expect that the
 438 result (50) should also give quantitative predictions for the finite XXZ chain in a certain
 439 regime. First of all, for the half-chain bipartition where the excitation is applied directly
 440 at the boundary, the role of the dispersion should not play an important role, as all the
 441 excitations can immediately enter the subsystem. Furthermore, one could argue that the

442 finite chain effectively corresponds to an interval of size $\ell = L$, which is the distance the
 443 quasiparticles have to cover before leaving the subsystem after reflection from the chain
 444 end. Clearly, the exact form of the plateau will not be the same in the two cases, but one
 445 expects the CFT results to be applicable in a regime $vt \ll L$. Finally, there is a highly
 446 nontrivial symmetry $s \rightarrow -s$ displayed by all the terms (51)-(53) in the expression of ΔS_2 ,
 447 corresponding to a change of the Luttinger parameter $K \rightarrow 1/K$, which is expected to
 448 be observed also in the lattice calculations. Note that since $K = 1$ corresponds to the
 449 free-fermion point $\Delta = 0$, the symmetry relates interaction strengths of different sign.

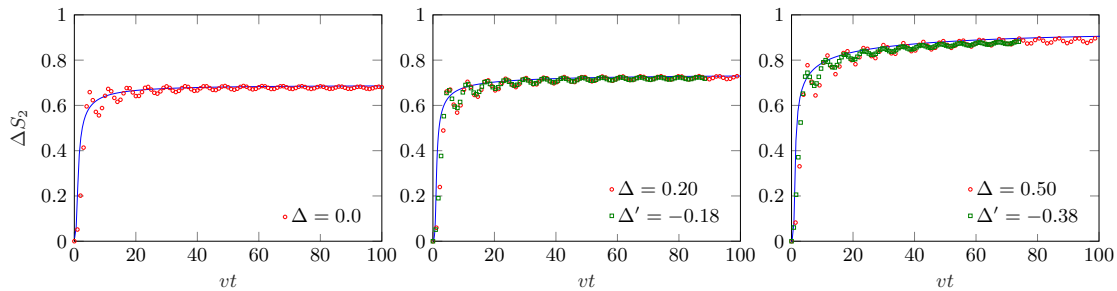


Figure 5: Growth of the Rényi entropy ΔS_2 for pairs of conjugate interaction parameters Δ and Δ' (red and green symbols) for a chain of length $L = 200$. The blue solid lines show the CFT result Eq. (50) with $\ell = 200$ and $d = 1$. The regularization $\epsilon = 0.55, 0.40, 0.35$ (from left to right) was tuned to obtain the best match with the tDMRG data.

450 In Fig. 5 we show a comparison of ΔS_2 obtained from tDMRG calculations for a XXZ
 451 chain with $L = 200$ divided in the middle, to the CFT result (50) shown by the blue
 452 solid lines. For the latter we have set $\ell = L$ and $d = 1$ as discussed above, whereas
 453 the regularization ϵ was set by hand in order to achieve the best agreement with the
 454 numerical data. One indeed observes that the CFT result gives, up to oscillations, a good
 455 quantitative description of the XXZ numerics. Furthermore, for each $\Delta \neq 0$, we also
 456 performed the calculation for the conjugate Δ' corresponding to $K' = 1/K$, leading to a
 457 remarkably good collapse of the curves.

458 5 Entanglement dynamics in the gapped phase

459 The CFT studies of the previous section give a rather good qualitative description of
 460 the entanglement spreading in the critical phase of the XXZ chain. To obtain a complete
 461 picture, in this section we shall study the dynamics in the gapped antiferromagnetic phase.
 462 For a physically motivated setting, we choose one of the symmetry-broken ground states
 463 $|\psi_\uparrow\rangle$ from Eq. (8), with a nonvanishing staggered magnetization (9). We now consider
 464 local Majorana operators, defined in terms of the spin variables as

$$\tilde{m}_{2j-1} = \left(\prod_{l=-L/2+1}^{j-1} \sigma_l^x \right) \sigma_j^z, \quad \tilde{m}_{2j} = \left(\prod_{l=-L/2+1}^{j-1} \sigma_l^x \right) \sigma_j^y. \quad (56)$$

465 Note that these operators differ from the ones in (22) discussed in the gapless phase by
 466 an interchange of the x and z spin components, but they also obey Majorana fermion
 467 statistics with anticommutation relations $\{\tilde{m}_k, \tilde{m}_l\} = 2\delta_{kl}$. We focus on the case of a
 468 domain wall created by \tilde{m}_1 in the center of the chain, which is then time evolved by the
 469 XXZ Hamiltonian (1)

$$|\psi(t)\rangle = e^{-iHt} \tilde{m}_1 |\psi_\uparrow\rangle. \quad (57)$$

470 Note that, in order to find the proper symmetry-broken ground state, in the DMRG
 471 simulation we add to the Hamiltonian a small staggered field in the z -direction, which is
 472 then decreased towards zero during the sweeps.

473 First we have a look at the entropy growth ΔS for the half-chain $r = 0$ as a function of
 474 time, shown on the left of Fig. 6 for several values of the anisotropy $\Delta > 1$. One observes
 475 a clear saturation of the excess entropy for large times, which is reached very quickly for
 476 large values of Δ . The asymptotic value of ΔS decreases with Δ and always exceeds $\ln(2)$.
 477 Remarkably, as shown on the right of Fig. 6, we find that the asymptotic excess entropy is
 478 well described by the formula $\Delta S = S(0) + \ln(2)$, where $S(0)$ is the ground-state entropy
 479 of the half-chain in the symmetry-broken state. Repeating the calculation for the excess
 480 Rényi entropy ΔS_2 , we find the exact same relation with $S_2(0)$.

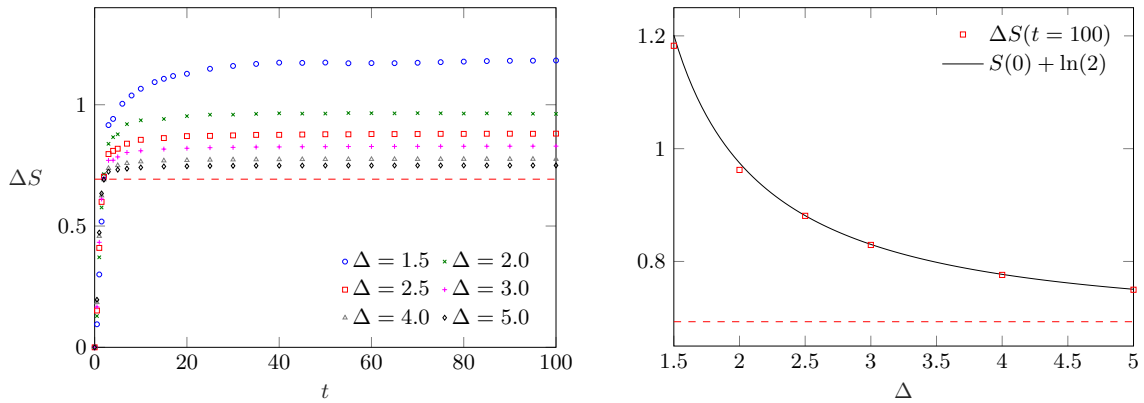


Figure 6: Left: Entanglement growth in the middle of the chain after a domain-wall excitation \tilde{m}_1 for different values of $\Delta > 1$ and $L = 400$. Right: ΔS at $t = 100$ compared to $S(0) + \ln(2)$ from Eq. (59). The red dashed line denotes $\ln(2)$. Note the different vertical scales.

481 To gain a deeper understanding of the above relation, one should invoke the exact
 482 results for the reduced density matrix of the half-chain, which can be found with the
 483 corner transfer matrix (CTM) method as [50]

$$\rho_A = \frac{e^{-H_{CTM}}}{\text{Tr}(e^{-H_{CTM}})}, \quad H_{CTM} = \sum_{j=0}^{\infty} \epsilon_j n_j, \quad (58)$$

484 where the single-particle eigenvalues are given by $\epsilon_j = 2j\phi$ with $\phi = \text{acosh}(\Delta)$, and $n_j =$
 485 $0, 1$ denotes fermionic occupation numbers. In other words, the entanglement Hamiltonian
 486 H_{CTM} of the ground state is characterized by an equispaced single-particle entanglement
 487 spectrum. Strictly speaking, this result applies to a half-infinite chain, but in practice it
 488 holds also for finite chains of length much larger than the correlation length. Note also,
 489 that the result (58) applies for the symmetric ground state, whereas for the symmetry-
 490 broken state the term $j = 0$ is missing from the sum. In that case, the von Neumann and
 491 Rényi entropies can be simply expressed as [51]

$$S(0) = \sum_{j=1}^{\infty} \left[\log \left(1 + e^{-2j\phi} \right) + \frac{2j\phi}{1 + e^{2j\phi}} \right], \quad (59)$$

492 as well as

$$S_n(0) = \frac{1}{1-n} \left[\sum_{j=1}^{\infty} \log \left(1 + e^{-2nj\phi} \right) - n \sum_{j=1}^{\infty} \log \left(1 + e^{-2j\phi} \right) \right]. \quad (60)$$

493 It is easy to see that the inclusion of the term $j = 0$ with $\epsilon_0 = 0$ simply yields an
 494 extra $\ln(2)$ contribution to the entropies. This change alone, however, would not explain
 495 our findings for the asymptotic excess entropy in Fig. 6, which seems to indicate that
 496 $S(t) \approx 2S(0) + \ln(2)$ for $t \gg 1$. Indeed, in order to obtain such a formula, one would
 497 have to add a double degeneracy for each ϵ_j with $j \neq 0$. Let us now discuss how such a
 498 degeneracy is reflected in the eigenvalues λ_l of the reduced density matrix. In fact, it is
 499 more convenient to introduce the scaled quantity

$$\nu_l = -\frac{1}{\phi} \ln \left(\frac{\lambda_l}{\lambda_0} \right), \quad (61)$$

500 where λ_0 denotes the maximal eigenvalue. For the initial symmetry-broken ground state,
 501 ν_l are independent of Δ and can only assume even integer values, with occasional multi-
 502 plicities due to different integer partitions. The lowest lying λ_l yield $\nu_l = 0, 2, 4, 6, 6, \dots$,
 503 i.e. the first degeneracy appears as $6 = 2 + 4$. The inclusion of the $\epsilon_0 = 0$ term simply
 504 gives an overall double degeneracy of the levels λ_l . The doubling of the ϵ_j for $j \neq 0$ further
 505 increases the degeneracies. Altogether, the combined effect would lead to the multiplicities
 506 $(2, 4, 6)$ for $\nu_l = 0, 2, 4$.

507 To check these predictions, in Fig. 7 we have plotted the 12 lowest lying ν_l calculated
 508 from the reduced density matrix eigenvalues, as obtained from tDMRG simulations after
 509 time evolving the state (57) to $t = 100$. One can see that the ν_l lie indeed rather close
 510 to the expected even integer values, approximately reproducing the expected multiplicity
 511 structure. Interestingly, the largest deviation around $\nu_l = 4$ is found for $\Delta = 5$, where
 512 one actually finds the best agreement with the entropy formula, see Fig. 6. In fact,
 513 however, the contribution of these eigenvalues to the entropy is already negligible. Note
 514 that the situation for larger values of ν_l is much less clear, as they correspond to very
 515 small eigenvalues λ_l which are already seriously affected by tDMRG truncation errors.

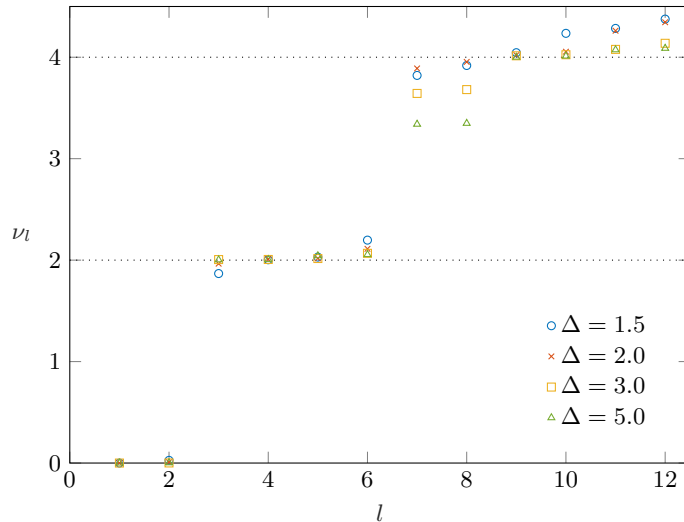


Figure 7: Scaled levels ν_l obtained from the reduced density matrix eigenvalues λ_l at time $t = 100$ via Eq. (61) for different Δ .

516 Although we find a nontrivial asymptotic behaviour of the half-chain entanglement,
 517 we expect that the full profile should still be described, up to a multiplicative factor, by
 518 the quasiparticle ansatz introduced in section 3.1, similarly to the Majorana excitation in

519 the gapless phase in Fig. 2. Therefore, we put forward the ansatz

$$\Delta S = \left(1 + \frac{S(0)}{\ln 2}\right) [-\mathcal{N} \ln(\mathcal{N}) - (1 - \mathcal{N}) \ln(1 - \mathcal{N})], \quad (62)$$

520 and for the excess Rényi entropy we propose

$$\Delta S_n = \left(1 + \frac{S_n(0)}{\ln 2}\right) \frac{1}{1-n} \ln[\mathcal{N}^n + (1 - \mathcal{N})^n]. \quad (63)$$

521 The quasiparticle fraction \mathcal{N} must now be evaluated via (16) by using the spinon velocities
 522 (13) in the gapped phase. Note that the binary entropy functions are multiplied by a factor
 523 to reproduce our findings for the half-chain, where $\mathcal{N} = 1/2$. The results of our numerical
 524 calculations for the profiles ΔS and ΔS_2 , plotted against the scaling variable $\zeta = r/t$, are
 525 shown in Fig. 8. The solid lines show the respective ansatz (62) and (63), which give a
 526 very good description of the data for both Δ values shown. In fact, we checked that the
 527 profiles are nicely reproduced even for $\Delta = 1.5$, which already corresponds to a relatively
 528 large correlation length.

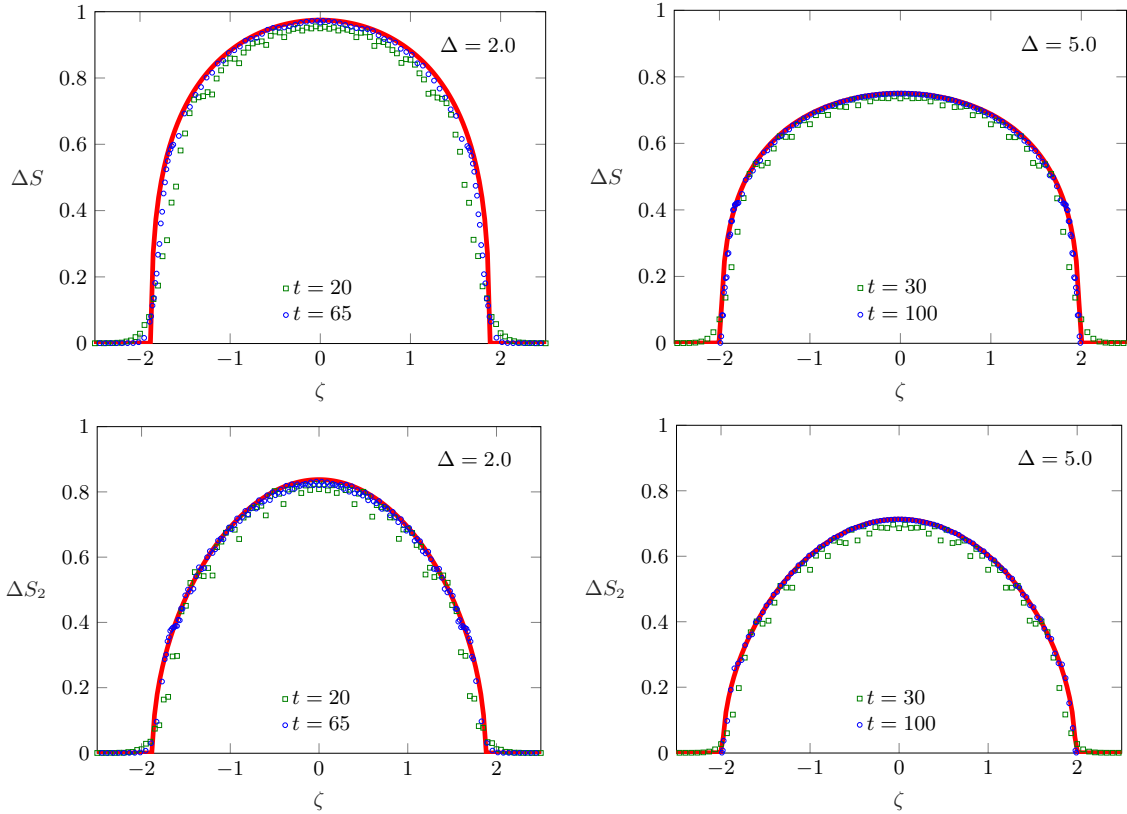


Figure 8: Entropy profiles ΔS (top) and ΔS_2 (bottom) after a domain-wall excitation \tilde{m}_1 for two different value of Δ and $L = 400$. The solid lines show the ansatz Eq. (62) for the von Neumann, as well as Eq. (63) for the $n = 2$ Rényi excess entropy.

529 5.1 Magnetization profiles

530 To conclude this section, we also investigate the spreading of the magnetization profiles
 531 for the antiferromagnetic domain wall excited by \tilde{m}_1 . This setting was studied previously
 532 with a focus on the edge behaviour of the profile [52]. In order to remove the dependence

533 on the ground-state value (9) of the staggered magnetization, we consider the normalized
 534 profile

$$\mathcal{M}_j(t) = \frac{\langle \psi(t) | \sigma_j^z | \psi(t) \rangle}{\langle \psi_\uparrow | \sigma_j^z | \psi_\uparrow \rangle}, \quad (64)$$

535 which then varies between $-1 \leq \mathcal{M}_j(t) \leq 1$ along the chain. We are mainly interested in
 536 the quasiparticle description of the time-evolved profile. In fact, a very similar problem
 537 was studied for a ferromagnetic domain wall in the XY chain [28], by first expanding
 538 the excited state in the single-particle basis of the Hamiltonian, which can then be time
 539 evolved trivially.

540 Here we assume that the dominant weight for our simple domain wall is carried by
 541 single-spinon excitations $|q\rangle$. Strictly speaking, this is only possible if one considers an-
 542 tiperiodic or open boundary conditions on the spins, since for a periodic chain spinons are
 543 created in pairs (i.e. one actually has a pair of domain walls). The time evolved state can
 544 then be written as

$$|\psi(t)\rangle \simeq \sum_q e^{-it\varepsilon_s(q)} c(q) |q\rangle, \quad (65)$$

545 where $\varepsilon_s(q)$ is the spinon dispersion (10), while $c(q)$ are the overlaps of the domain-wall
 546 excitation with the single-spinon states. Note that the momentum of a single spinon satis-
 547 fies $0 \leq q \leq \pi$, however, the total momentum of spinons above the quasidegenerate ground
 548 state is shifted by π . Since the domain wall is created by a strictly local fermionic opera-
 549 tor, we assume that in the thermodynamic limit $|c(q)|$ becomes a constant in momentum
 550 space, i.e. $c(q) = e^{i\alpha(q)}/\sqrt{N}$ is just a phase factor normalized by the number N of spinon
 551 states. Using this in (65), one obtains for the profile

$$\mathcal{M}_j(t) = \frac{1}{N} \sum_p \sum_q e^{-it(\varepsilon_s(q) - \varepsilon_s(p))} e^{i(\alpha(q) - \alpha(p))} \frac{\langle p | \sigma_j^z | q \rangle}{\langle \psi_\uparrow | \sigma_j^z | \psi_\uparrow \rangle}. \quad (66)$$

552 Clearly, the main difficulty of calculating (66) is due to the form factors $\langle p | \sigma_j^z | q \rangle$. For
 553 the transverse Ising and XY chains, such form factors are known explicitly [53, 54] and
 554 were used to obtain a double integral representation of the magnetization profile [26, 28].
 555 The hydrodynamic limit can then be obtained from the stationary-phase analysis of the
 556 integrals. Moreover, there exists a number of form factor results for the XXZ chain as well
 557 (see e.g. [55, 56]), which were used in numerical studies of the magnetization profile after
 558 a spin-flip excitation [57]. Unfortunately, however, the expressions are typically rather
 559 involved or not in a representation that could be useful for our purposes. In fact, we are
 560 not aware of any results where the required single-spinon matrix elements are evaluated
 561 as a function of the spinon rapidity or momentum.

562 Nevertheless, based on the known results, we give a handwaving argument about how
 563 the main structure of the form factor should look like. Most importantly, we assume that
 564 it becomes singular for $p \rightarrow q$ and can be written as

$$\lim_{p \rightarrow q} \frac{\langle p | \sigma_j^z | q \rangle}{\langle \psi_\uparrow | \sigma_j^z | \psi_\uparrow \rangle} \simeq \frac{i}{N} e^{i(q-p)j} \frac{\mathcal{F}(q)}{p-q}. \quad (67)$$

565 Here the only j -dependence is in the exponential factor that follows from the action of
 566 the translation operator, and the function $\mathcal{F}(q)$ denotes the slowly varying part of the
 567 form factor around its pole. The factor $1/N$ is required for a proper thermodynamic limit
 568 of (66). Converting the sums into integrals, one can proceed with the stationary phase
 569 analysis similarly to the XY case [28], by expanding the phases around $Q = q - p = 0$.
 570 Using a resolution of the pole and the definition of the step function

$$\frac{1}{Q} = i\pi\delta(Q) + \lim_{\epsilon \rightarrow 0} \frac{1}{Q + i\epsilon}, \quad \Theta(x) = - \lim_{\epsilon \rightarrow 0} \int_{-\infty}^{\infty} \frac{dQ}{2\pi i} \frac{e^{-iQx}}{Q + i\epsilon}, \quad (68)$$

571 one arrives at the following simple expression for the profile

$$\mathcal{M}_j(t) = 1 - 2\tilde{\mathcal{N}}, \quad \tilde{\mathcal{N}} = \int_0^\pi \frac{dq}{\pi} \Theta(v_s(q)t - j) \mathcal{F}(q). \quad (69)$$

572 Note that the proper normalization of the profile for $t = 0$ requires to have

$$\int_0^\pi \frac{dq}{\pi} \mathcal{F}(q) = 1. \quad (70)$$

573 The result (69) is nothing else but the quasiparticle interpretation of the magnetization
 574 profile in the hydrodynamic limit. Indeed, the initial sharp domain wall is carried away by
 575 spinons of different momenta q and velocities $v_s(q)$, where $\mathcal{F}(q)$ gives the corresponding
 576 weight. Unfortunately, without an explicit analytical result on the form factor, one has to
 577 make a guess on the weight function. The simplest assumption is $\mathcal{F}(q) \equiv 1$, which indeed
 578 holds true for the XY chain form factors [28]. With this simple choice one actually has
 579 $\tilde{\mathcal{N}} = \mathcal{N}$, that is we recover the spinon fraction introduced in (16) for the description of
 580 the entropy profile. In Fig. 9 we show the comparison of this simple ansatz to the tDMRG
 581 data, with a rather good agreement for a large $\Delta = 5$. For $\Delta = 2$, however, one can
 582 already see the deviations from our simple ansatz, which fails completely for even smaller
 583 anisotropies. Thus, in sharp contrast to the case of the entanglement entropies, the spinon
 584 contributions to the magnetization cannot be taken to be equal, except for close to the
 585 Ising limit.

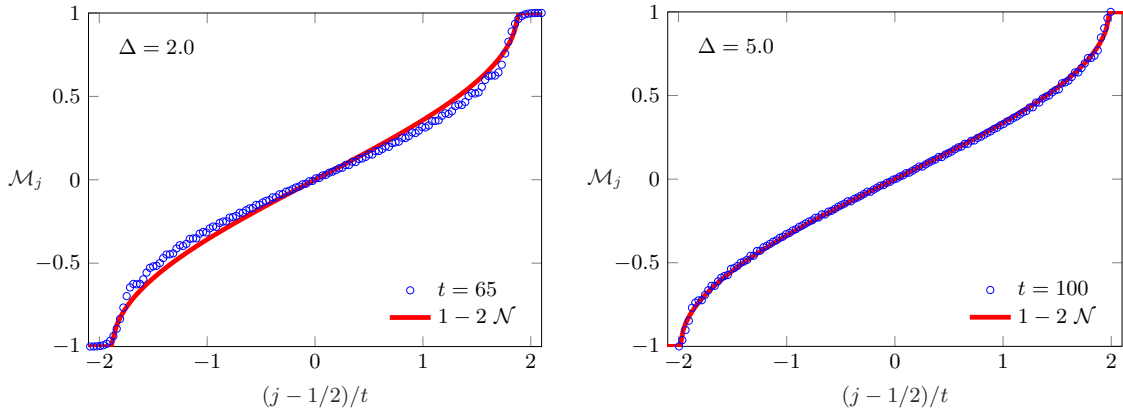


Figure 9: Normalized magnetization profiles $\mathcal{M}_j(t)$ obtained from tDMRG calculations for $\Delta = 2.0$ (left) and $\Delta = 5.0$ (right) after a domain-wall excitation \tilde{m}_1 in a chain of length $L = 400$. The solid lines show the ansatz $1 - 2\mathcal{N}$, with the spinon fraction Eq. (16) calculated from the velocities in Eq. (13).

586 6 Summary and discussion

587 We studied the entanglement spreading in the XXZ chain after excitations that are strictly
 588 local in terms of the fermion operators. In the gapless phase we found that the time evolu-
 589 tion after a fermion creation operator yields an entropy profile that can be well described
 590 by a probabilistic quasiparticle ansatz for not too large Δ , assuming equal contributions
 591 from low-lying spinon excitations. On the other hand, for a local Majorana excitation we
 592 observe that the quasiparticle ansatz holds only up to a multiplicative factor, determined
 593 by the excess entropy at the operator insertion point. This is in agreement with our CFT

594 calculations, which suggest that the excess entropy exceeds $\ln(2)$ for any $\Delta \neq 0$, with
 595 a very slow convergence towards the asymptotic value $2\ln(2)$. In the symmetry-broken
 596 gapped phase we considered a different Majorana excitation, creating an antiferromag-
 597 netic domain wall. For the entropy profile we find again a nontrivial prefactor, whereas
 598 our simple ansatz for the magnetization, assuming equal contributions from the spinons,
 599 holds only in the Ising limit $\Delta \rightarrow \infty$.

600 The main limitation of our quasiparticle ansatz (17) is that it includes only the low-
 601 lying spinons. It is natural to ask how well such an assumption actually holds for our local
 602 excitations in the different regimes. A simple way to quantify the spectral weight of the
 603 spinons in the gapless regime is via the energy difference $\langle \Delta E \rangle = \langle \psi_0 | (m_1 H m_1 - H) | \psi_0 \rangle$
 604 of the Majorana excitation (equal to that of c_1^\dagger by particle-hole symmetry) measured from
 605 the ground state, whereas in the gapped case we replace $m_1 \rightarrow \tilde{m}_1$. Our assumption in
 606 both regimes was that one can practically work with single-spinon states, whose energies
 607 above the ground state are given by the corresponding dispersions $\varepsilon_s(q)$ in (4) and (10),
 608 respectively. This yields the simple formula for the energy difference

$$\langle \Delta E \rangle = \int_0^\pi \varepsilon_s(q) \frac{dq}{\pi}. \quad (71)$$

609 To test the validity of our assumption, in Fig. 10 we compare the energy difference
 610 obtained from DMRG to the formula (71) in both gapless and gapped phases. As expected,
 611 the result at the free-fermion point $\Delta = 0$ is exactly reproduced, while the error remains
 612 relatively small in the regime $|\Delta| \lesssim 0.5$. However, not surprisingly, the overall behaviour
 613 of $\langle \Delta E \rangle$ is not properly captured by the naive ansatz (71), especially for $\Delta \rightarrow -1$, which
 614 is exactly what we observed for the entropy profiles in Fig. 1. On the other hand, in the
 615 gapped phase shown on the right of Fig. 10, one has a qualitatively good description in
 616 the entire regime, with the error decreasing for $\Delta \gg 1$. This explains why we had a much
 617 better overall description of the entropy profiles for $\Delta > 1$ via the quasiparticle ansatz
 618 (62).

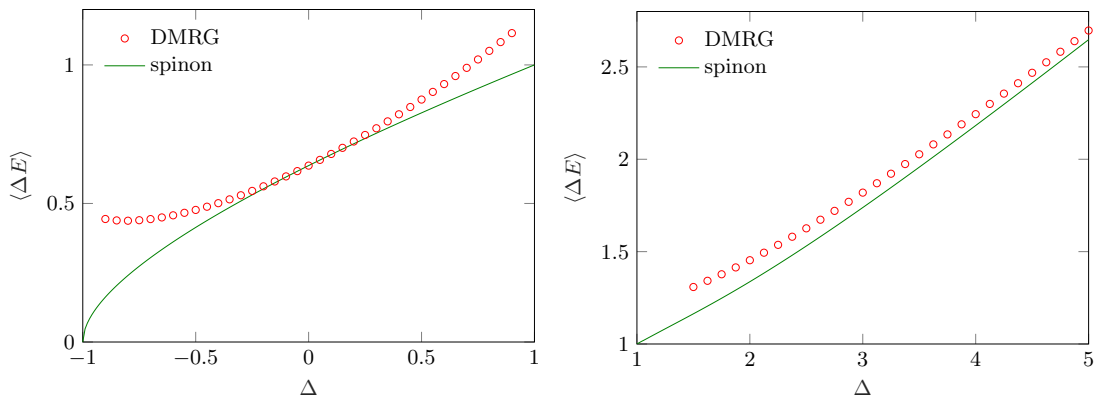


Figure 10: Energy difference due to the insertion of local operator m_1 in the gapless (left) and \tilde{m}_1 in the gapped (right) regime. DMRG results (symbols) for $L = 400$ are compared to the spinon ansatz (lines) in Eq. (71). Note the different vertical scales.

619 Another feature that is not completely understood is the multiplicative factor of the
 620 spinon ansatz appearing for Majorana excitations. In the gapless phase this could be
 621 accounted for the mixing of the chiral boson modes and yields a factor 2 in the limit $t \rightarrow \infty$
 622 for any $\Delta \neq 0$. The exceptional behaviour of the XX chain can actually be also understood
 623 directly, using a duality transformation [58–61] that relates it to two independent and
 624 critical transverse Ising chains. Furthermore, as shown in [26], the Majorana excitation on

625 the XX chain transforms under the dual map into a Majorana excitation acting only on a
 626 *single* Ising chain. Hence, the asymptotic excess entropy is given by $\ln(2)$ and there is no
 627 doubling in this case. On the other hand, in the gapped phase the prefactor in (62) seems
 628 to be nontrivially related to the ground-state entanglement entropy. Note that a similar
 629 observation was reported after a local quench in the non-critical transverse Ising chain [62],
 630 where the entanglement plateau was also found to be related to the ground-state value.
 631 A deeper understanding of these effects requires further studies.

632 Finally, let us comment about the case where the locality of the excitation is not
 633 imposed in the fermionic but rather in the spin picture. In other words, instead of the
 634 c_j^\dagger excitation one could consider the spin operator σ_j^+ by dropping the Jordan-Wigner
 635 string in (19). According to our tDMRG calculations carried out for this case, the entropy
 636 profiles change completely, becoming more flat in the center with a maximum that stays
 637 way below $\ln(2)$. In short, the fermionic nature of the local excitations turns out to be
 638 essential for the applicability of the quasiparticle description.

639 Acknowledgements

640 The authors acknowledge funding from the Austrian Science Fund (FWF) through project
 641 No. P30616-N36.

642 A Correlation functions of vertex operators

643 In the following we give the main steps of the calculation of the excess Rényi entropy ΔS_2 ,
 644 obtained via the ratio (34) of four-point and two-point functions. As in the main text, we
 645 consider two different local operators, the one corresponding to the fermion creation

$$\mathcal{O}_f = e^{ik_F d} \psi^\dagger + e^{-ik_F d} \bar{\psi}^\dagger, \quad (72)$$

646 as well as the Hermitian Majorana excitation

$$\mathcal{O}_m = e^{ik_F d} \psi^\dagger + e^{-ik_F d} \bar{\psi}^\dagger + e^{-ik_F d} \psi + e^{ik_F d} \bar{\psi}. \quad (73)$$

647 They are composed of chiral fermion fields which, after the Bogoliubov transformation (41),
 648 can be written as vertex operators (42) involving chiral boson fields. The holomorphic and
 649 anti-holomorphic components of the vertex operators are summarized in the table below,
 where $c = \cosh(\xi)$ and $s = \sinh(\xi)$.

	ψ	ψ^\dagger	$\bar{\psi}$	$\bar{\psi}^\dagger$
α	$-c$	c	s	$-s$
β	$-s$	s	c	$-c$

Table 1: Parameters of the vertex operators (42) for the fermionic fields

650 We start by evaluating the two point function in the denominator of (34). Using
 651 the fact that vertex operators are primaries with conformal dimensions $h = \alpha^2/2$ and
 652 $\bar{h} = \beta^2/2$, one immediately obtains the nonvanishing two-point functions on the plane as
 653

$$\begin{aligned} \langle \psi(w_1, \bar{w}_1) \psi^\dagger(w_2, \bar{w}_2) \rangle &\propto (w_1 - w_2)^{-c^2} (\bar{w}_1 - \bar{w}_2)^{-s^2}, \\ \langle \bar{\psi}(w_1, \bar{w}_1) \bar{\psi}^\dagger(w_2, \bar{w}_2) \rangle &\propto (w_1 - w_2)^{-s^2} (\bar{w}_1 - \bar{w}_2)^{-c^2}. \end{aligned} \quad (74)$$

654 From (32) we have $w_1 - w_2 = \bar{w}_1 - \bar{w}_2 = 2\epsilon$, thus we obtain for the two-point functions

$$\langle \mathcal{O}_f^\dagger(w_1, \bar{w}_1) \mathcal{O}_f(w_2, \bar{w}_2) \rangle = 2(2\epsilon)^{-(c^2+s^2)}, \quad \langle \mathcal{O}_m^\dagger(w_1, \bar{w}_1) \mathcal{O}_m(w_2, \bar{w}_2) \rangle = 4(2\epsilon)^{-(c^2+s^2)}. \quad (75)$$

655 Let us now move to the four-point function on the Riemann surface Σ_2 . This is a
656 sum of many terms, from which the nonvanishing contributions allowed by the neutrality
657 conditions (44) are given by

$$\langle \psi \psi^\dagger \bar{\psi} \bar{\psi}^\dagger \rangle, \quad \langle \bar{\psi} \bar{\psi}^\dagger \psi \psi^\dagger \rangle, \quad \langle \bar{\psi} \psi^\dagger \psi \bar{\psi}^\dagger \rangle, \quad \langle \psi \bar{\psi}^\dagger \bar{\psi} \psi^\dagger \rangle, \quad \langle \psi \psi^\dagger \psi \psi^\dagger \rangle, \quad \langle \bar{\psi} \bar{\psi}^\dagger \bar{\psi} \bar{\psi}^\dagger \rangle. \quad (76)$$

658 We first analyze the Jacobian of the transformation (38) from $\Sigma_2 \rightarrow \Sigma_1$. The derivatives
659 of the mapping are given by

$$\frac{dw}{dz} = i\ell \frac{nz^{n-1}}{(1-z^n)^2}, \quad \frac{d\bar{w}}{d\bar{z}} = -i\ell \frac{n\bar{z}^{n-1}}{(1-\bar{z}^n)^2}. \quad (77)$$

660 Introducing the variable

$$\chi = \frac{(1-z_1^2)^2(1-z_2^2)^2}{4z_1z_2}, \quad (78)$$

661 one obtains for the first four contributions in (76)

$$\ell^{-2(c^2+s^2)} \chi^{c^2/2} \bar{\chi}^{s^2/2} \chi^{s^2/2} \bar{\chi}^{c^2/2} = \ell^{-2(c^2+s^2)} |\chi|^{c^2+s^2}, \quad (79)$$

662 whereas for the last two contributions we have, respectively

$$\ell^{-2(c^2+s^2)} \chi^{c^2} \bar{\chi}^{s^2}, \quad \ell^{-2(c^2+s^2)} \chi^{s^2} \bar{\chi}^{c^2}. \quad (80)$$

663 Note that there is an extra sign factor $(-i)^{c^2} (i)^{s^2} (i)^{s^2} (-i)^{c^2} = (-i)^{2(c^2-s^2)} = -1$ which
664 multiplies the first two Jacobian.

665 The next step is to evaluate the vertex four-point functions. Using (43) this reads for
666 the first term in (76)

$$z_{12}^{-c^2} z_{34}^{-s^2} z_{13}^{-cs} z_{24}^{-cs} z_{14}^{cs} z_{23}^{cs} z_{12}^{-s^2} z_{34}^{-c^2} z_{13}^{-cs} z_{24}^{-cs} z_{14}^{cs} z_{23}^{cs} = (-1) |1-\eta|^{2cs} |\eta|^{-(c^2+s^2)} |z_{13}z_{24}|^{-(c^2+s^2)} \quad (81)$$

667 Note that we have used the property $z_{34} = -z_{12}$. It is easy to check that one obtains the
668 very same factor from the second term. Similarly, using $z_{23} = z_{14}$, one can check that the
669 third and fourth terms deliver

$$z_{12}^{cs} z_{34}^{cs} z_{13}^{-cs} z_{24}^{-cs} z_{14}^{-c^2} z_{23}^{-s^2} z_{12}^{cs} z_{34}^{-cs} z_{13}^{-cs} z_{24}^{-cs} z_{14}^{-s^2} z_{23}^{-c^2} = |\eta|^{2cs} |1-\eta|^{-(c^2+s^2)} |z_{13}z_{24}|^{-(c^2+s^2)}. \quad (82)$$

670 For the fifth term one has

$$[\eta(1-\eta)]^{-c^2} (z_{13}z_{24})^{-c^2} [\bar{\eta}(1-\bar{\eta})]^{-s^2} (\bar{z}_{13}\bar{z}_{24})^{-s^2}, \quad (83)$$

671 and the last term follows by interchanging c and s above.

672 In order to obtain an expression in terms of the cross-ratios, one can rewrite (78) as

$$\chi = \left(\frac{\ell}{2\epsilon} \right)^2 \eta(1-\eta) z_{13}z_{24}. \quad (84)$$

673 Putting everything together, one arrives at the four-point function

$$2(2\epsilon)^{-2(c^2+s^2)} \left[|\eta|^{(c+s)^2} + |1-\eta|^{(c+s)^2} + 1 \right]. \quad (85)$$

674 Evaluating the four-point function for the Majorana excitation (73) is more cumbersome, since one has a large number of terms to consider. There are, however, some simple
 675 rules and symmetry arguments which make the task easier. First of all, one should clearly
 676 always have the same number of creation and annihilation operators, for the neutrality
 677 conditions (44) of the vertex correlation functions to be satisfied. This already drastically
 678 reduces the number of terms to consider. The remaining ones can be collected into
 679 families, some of them given by (76).

681 Let us consider the family generated by the first term in (76), by allowing permutations
 682 of the left- and right-moving operators separately (i.e. interchanging the first or last two
 683 operators). If only the first or last two are interchanged, the vertex correlator (81) is
 684 modified by replacing

$$|1 - \eta|^{2cs} \rightarrow |1 - \eta|^{-2cs}, \quad (86)$$

685 whereas the correlator remains the same if both of them are interchanged. The next
 686 family is generated by the second term in (76), which is actually related to the first one by
 687 Hermitian conjugation. Hence this just gives a factor of two. The same argument holds
 688 for the next two families, where interchanging only one pair modifies the correlator in (82)
 689 as

$$|\eta|^{2cs} \rightarrow |\eta|^{-2cs}. \quad (87)$$

690 Finally, the single interchange in the fifth family leads to

$$(1 - \eta)^{-c^2} \rightarrow (1 - \eta)^{c^2}, \quad (1 - \bar{\eta})^{-s^2} \rightarrow (1 - \bar{\eta})^{s^2}, \quad (88)$$

691 whereas the last family follows by interchanging c and s above.

692 There are, however, two additional families appearing where the left- and right-moving
 693 particles are intertwined. They are given by the representative correlators

$$\langle \psi \bar{\psi}^\dagger \psi^\dagger \bar{\psi} \rangle, \quad \langle \bar{\psi} \psi^\dagger \bar{\psi}^\dagger \psi \rangle. \quad (89)$$

694 Defining the variable

$$\sigma = \frac{(1 - z_1^2)^2 (1 - \bar{z}_2^2)^2}{4z_1 \bar{z}_2}, \quad (90)$$

695 the corresponding Jacobians contain the factors $\sigma^{c^2} \bar{\sigma}^{s^2}$ and $\sigma^{s^2} \bar{\sigma}^{c^2}$, respectively. Further-
 696 more, the vertex correlation functions yield

$$|\eta|^{\pm 2cs} |1 - \eta|^{\mp 2cs} (z_{13} \bar{z}_{24})^{-c^2} (\bar{z}_{13} z_{24})^{-s^2}, \quad |\eta|^{\pm 2cs} |1 - \eta|^{\mp 2cs} (z_{13} \bar{z}_{24})^{-s^2} (\bar{z}_{13} z_{24})^{-c^2}, \quad (91)$$

697 and each term comes with a double multiplicity. Collecting all the terms, the four-point
 698 function takes the form

$$2 (2\epsilon)^{-2(c^2+s^2)} (2A + B + C), \quad (92)$$

699 where the factors A , B and C are reported in (51)-(53).

700 References

- 701 [1] P. Calabrese, F. H. L. Essler and G. Mussardo, *Introduction to 'Quantum Integrability*
 702 *in Out of Equilibrium Systems'*, J. Stat. Mech. 064001 (2016), doi:10.1088/1742-
 703 5468/2016/06/064001.
- 704 [2] A. Polkovnikov, K. Sengupta, A. Silva and M. Vengalattore, *Nonequilibrium dy-*
 705 *namics of closed interacting quantum systems*, Rev. Mod. Phys. **83**, 863 (2011),
 706 doi:10.1103/RevModPhys.83.863.

- 707 [3] C. Gogolin and J. Eisert, *Equilibration, thermalisation, and the emergence of sta-*
708 *tistical mechanics in closed quantum systems*, Rep. Prog. Phys. **79**, 056001 (2016),
709 doi:10.1088/0034-4885/79/5/056001.
- 710 [4] L. Vidmar and M. Rigol, *Generalized Gibbs ensemble in integrable lattice models*, J.
711 Stat. Mech. 064007 (2016), doi:10.1088/1742-5468/2016/06/064007.
- 712 [5] J. Eisert, M. Cramer and M. B. Plenio, *Area laws for the entanglement entropy*, Rev.
713 Mod. Phys. **82** (2010), doi:10.1103/RevModPhys.82.277.
- 714 [6] F. H. L. Essler and M. Fagotti, *Quench dynamics and relaxation in isolated in-*
715 *tegrable quantum spin chains*, J. Stat. Mech. 064002 (2016), doi:10.1088/1742-
716 5468/2016/06/064002.
- 717 [7] P. Calabrese and J. L. Cardy, *Evolution of entanglement entropy in one-dimensional*
718 *systems*, J. Stat. Mech. P04010 (2005), doi:10.1088/1742-5468/2005/04/P04010.
- 719 [8] V. Alba and P. Calabrese, *Entanglement and thermodynamics after a quan-*
720 *tum quench in integrable systems*, Proc. Natl. Acad. Sci. **114**, 7947 (2017),
721 doi:10.1073/pnas.1703516114.
- 722 [9] V. Alba and P. Calabrese, *Entanglement dynamics after quantum quenches in generic*
723 *integrable systems*, SciPost Phys. **4**, 017 (2018), doi:10.21468/SciPostPhys.4.3.017.
- 724 [10] P. Calabrese, *Entanglement spreading in non-equilibrium integrable systems*, URL
725 <https://arxiv.org/abs/2008.11080>, ArXiv:2008.11080 (2020).
- 726 [11] P. Calabrese and J. Cardy, *Entanglement and correlation functions following a*
727 *local quench: a conformal field theory approach*, J. Stat. Mech. P10004 (2007),
728 doi:10.1088/1742-5468/2007/10/p10004.
- 729 [12] P. Calabrese and J. Cardy, *Quantum quenches in 1+1 dimensional conformal field*
730 *theories*, J. Stat. Mech. 064003 (2016).
- 731 [13] J.-M. Stéphan and J. Dubail, *Local quantum quenches in critical one-dimensional*
732 *systems: entanglement, the Loschmidt echo, and light-cone effects*, J. Stat. Mech.
733 P08019 (2011), doi:10.1088/1742-5468/2011/08/P08019.
- 734 [14] V. Eisler and I. Peschel, *Evolution of entanglement after a local quench*, J. Stat.
735 Mech. P06005 (2007), doi:10.1088/1742-5468/2007/06/P06005.
- 736 [15] M. Nozaki, T. Numasawa and T. Takayanagi, *Quantum entanglement of lo-*
737 *cal operators in conformal field theories*, Phys. Rev. Lett. **112**, 111602 (2014),
738 doi:10.1103/PhysRevLett.112.111602.
- 739 [16] S. He, T. Numasawa, T. Takayanagi and K. Watanabe, *Quantum dimension as*
740 *entanglement entropy in two dimensional conformal field theories*, Phys. Rev. D **90**,
741 041701 (2014), doi:10.1103/PhysRevD.90.041701.
- 742 [17] M. Nozaki, *Notes on quantum entanglement of local operators*, J. High Energy Phys.
743 **2014**, 147 (2014), doi:10.1007/JHEP10(2014)147.
- 744 [18] M. Nozaki, T. Numasawa and S. Matsuura, *Quantum entanglement of fermionic local*
745 *operators*, J. High Energy Phys. **2016**, 150 (2016), doi:10.1007/JHEP02(2016)150.
- 746 [19] P. Caputa and A. Veliz-Orsorio, *Entanglement constant for conformal families*, Phys.
747 Rev. D **92**, 065010 (2015), doi:10.1103/PhysRevD.92.065010.

- 748 [20] B. Chen, W. Gui, S. He and J.-q. Wu, *Entanglement entropy for descen-*
749 *dent local operators in 2D CFTs*, J. High Energy Phys. **2015**, 173 (2015),
750 doi:10.1007/JHEP10(2015)173.
- 751 [21] W. Guo, S. He and Z. Luo, *Entanglement entropy in (1+1)D CFTs with multiple local*
752 *excitations*, J. High Energy Phys. **2018**, 154 (2018), doi:10.1007/JHEP05(2018)154.
- 753 [22] P. Caputa, J. Simón, A. Štikonas and T. Takayanagi, *Quantum entanglement of*
754 *localized excited states at finite temperature*, J. High Energy Phys. **2015**, 102 (2015),
755 doi:10.1007/JHEP01(2015)102.
- 756 [23] W. Guo and S. He, *Rényi entropy of locally excited states with thermal*
757 *and boundary effect in 2D CFTs*, J. High Energy Phys. **2015**, 99 (2015),
758 doi:10.1007/JHEP04(2015)099.
- 759 [24] P. Caputa and M. M. Rams, *Quantum dimensions from local operator excitations*
760 *in the Ising model*, J. Phys. A: Math. Theor. **50**, 055002 (2017), doi:10.1088/1751-
761 8121/aa5202.
- 762 [25] J. Zhang and P. Calabrese, *Subsystem distance after a local operator quench*, J. High
763 Energy Phys. **56** (2020), doi:10.1007/JHEP02(2020)056.
- 764 [26] V. Eisler, F. Maislinger and H. G. Evertz, *Universal front propagation in the*
765 *quantum Ising chain with domain-wall initial states*, SciPost Phys. **1**, 014 (2016),
766 doi:10.21468/SciPostPhys.1.2.014.
- 767 [27] V. Eisler and F. Maislinger, *Hydrodynamical phase transition for domain-wall melting*
768 *in the XY chain*, Phys. Rev. B **98**, 161117 (2018), doi:10.1103/PhysRevB.98.161117.
- 769 [28] V. Eisler and F. Maislinger, *Front dynamics in the XY chain after local excitations*,
770 SciPost Phys. **8**, 37 (2020), doi:10.21468/SciPostPhys.8.3.037.
- 771 [29] M. Takahashi, *Thermodynamics of One-Dimensional Solvable Models*, Cambridge
772 University Press (1999).
- 773 [30] F. Franchini, *An Introduction to Integrable Techniques for One-Dimensional Quan-*
774 *tum Systems*, vol. Lecture Notes in Physics Vol. 940, Springer (2017).
- 775 [31] S. R. White, *Density matrix formulation for quantum renormalization groups*, Phys.
776 Rev. Lett. **69**, 2863 (1992), doi:10.1103/PhysRevLett.69.2863.
- 777 [32] S. R. White, *Density-matrix algorithms for quantum renormalization groups*, Phys.
778 Rev. B **48**, 10345 (1993), doi:10.1103/PhysRevB.48.10345.
- 779 [33] U. Schollwöck, *The density-matrix renormalization group in the age of matrix product*
780 *states*, Ann. Phys. **326**, 96 (2011), doi:10.1016/j.aop.2010.09.012.
- 781 [34] A. L. de Paula, H. Bragança, R. G. Pereira, R. C. Drumond and M. C. O. Aguiar,
782 *Spinon and bound-state excitation light cones in Heisenberg XXZ chains*, Phys. Rev.
783 B **95**, 045125 (2017), doi:10.1103/PhysRevB.95.045125.
- 784 [35] R. Baxter, *Spontaneous staggered polarization of the F-model*, J. Stat. Phys. **9**, 145
785 (1973), doi:10.1007/BF01016845.
- 786 [36] A. Izergin, N. Kitanine, J. Maillet and V. Terras, *Spontaneous magnetization of the*
787 *XXZ Heisenberg spin-1/2 chain*, Nucl. Phys. B **554**, 679 (1999), doi:10.1016/S0550-
788 3213(99)00273-4.

- 789 [37] V. Alba, M. Fagotti and P. Calabrese, *Entanglement entropy of excited states*, J.
790 Stat. Mech. P10020 (2009), doi:10.1088/1742-5468/2009/10/p10020.
- 791 [38] J. Mölter, T. Barthel, U. Schollwöck and V. Alba, *Bound states and entangle-*
792 *ment in the excited states of quantum spin chains*, J. Stat. Mech. P10029 (2014),
793 doi:10.1088/1742-5468/2014/10/p10029.
- 794 [39] F. C. Alcaraz, M. I. Berganza and G. Sierra, *Entanglement of Low-Energy*
795 *Excitations in Conformal Field Theory*, Phys. Rev. Lett. **106**, 201601 (2011),
796 doi:10.1103/PhysRevLett.106.201601.
- 797 [40] M. I. Berganza, F. C. Alcaraz and G. Sierra, *Entanglement of excited states in critical*
798 *spin chains*, J. Stat. Mech. P01016 (2012), doi:10.1088/1742-5468/2012/01/p01016.
- 799 [41] O. A. Castro-Alvaredo, C. De Fazio, B. Doyon and I. M. Szécsényi, *Entangle-*
800 *ment Content of Quasiparticle Excitations*, Phys. Rev. Lett. **121**, 170602 (2018),
801 doi:10.1103/PhysRevLett.121.170602.
- 802 [42] O. A. Castro-Alvaredo, C. De Fazio, B. Doyon and I. M. Szécsényi, *Entanglement*
803 *content of quantum particle excitations. Part I. Free field theory*, J. High Energy
804 Phys. **2018**, 39 (2018), doi:10.1007/JHEP10(2018)039.
- 805 [43] S. R. White and A. E. Feiguin, *Real-Time Evolution Using the Den-*
806 *sity Matrix Renormalization Group*, Phys. Rev. Lett. **93**, 076401 (2004),
807 doi:10.1103/PhysRevLett.93.076401.
- 808 [44] A. J. Daley, C. Kollath, U. Schollwöck and G. Vidal, *Time-dependent density-matrix*
809 *renormalization-group using adaptive effective Hilbert spaces*, J. Stat. Mech. P04005
810 (2004), doi:10.1088/1742-5468/2004/04/p04005.
- 811 [45] M. Fishman, S. R. White and E. M. Stoudenmire, *The ITensor software library for*
812 *tensor network calculations* (2020), 2007.14822.
- 813 [46] D. Sénéchal, *An introduction to bosonization*, Springer, New York (2004).
- 814 [47] T. Giamarchi, *Quantum Physics in One Dimension*, Clarendon Press, Oxford (2003).
- 815 [48] P. Calabrese and J. Cardy, *Entanglement entropy and conformal field theory*, J. Phys.
816 A: Math. Theor. **42**, 504005 (2009), doi:10.1088/1751-8113/42/50/504005.
- 817 [49] P. Francesco, P. Mathieu and D. Sénéchal, *Conformal Field Theory*, Springer, New
818 York (1997).
- 819 [50] I. Peschel, M. Kaulke and O. Legeza, *Density-matrix spectra for integrable mod-*
820 *els*, Ann. Phys. **8**, 153 (1999), doi:10.1002/(SICI)1521-3889(199902)8:2<153::AID-
821 ANDP153>3.0.CO;2-N.
- 822 [51] P. Calabrese, J. Cardy and I. Peschel, *Corrections to scaling for block entangle-*
823 *ment in massive spin chains*, J. Stat. Mech. P09003 (2010), doi:10.1088/1742-
824 5468/2010/09/p09003.
- 825 [52] V. Zauner, M. Ganahl, H. G. Evertz and T. Nishino, *Time evolution within a comov-*
826 *ing window: scaling of signal fronts and magnetization plateaus after a local quench in*
827 *quantum spin chains*, J. Phys.: Condens. Matter **27**, 425602 (2015), doi:10.1088/0953-
828 8984/27/42/425602.

- 829 [53] N. Iorgov, V. Shadura and Y. Tykhyy, *Spin operator matrix elements in the quantum*
830 *Ising chain: fermion approach*, J. Stat. Mech. P02028 (2011), doi:10.1088/1742-
831 5468/2011/02/p02028.
- 832 [54] N. Iorgov, *Form factors of the finite quantum XY-chain*, J. Phys. A: Math. Theor.
833 **44**, 335005 (2011), doi:10.1088/1751-8113/44/33/335005.
- 834 [55] N. Kitanine, J. Maillet and V. Terras, *Form factors of the XXZ Heisenberg spin-1/2*
835 *finite chain*, Nucl. Phys. B **554**, 647 (1999), doi:10.1016/S0550-3213(99)00295-3.
- 836 [56] M. Dugave, F. Göhmann, K. K. Kozłowski and J. Suzuki, *On form-factor expan-*
837 *sions for the XXZ chain in the massive regime*, J. Stat. Mech. P05037 (2015),
838 doi:10.1088/1742-5468/2015/05/p05037.
- 839 [57] R. Vlijm and J.-S. Caux, *Spinon dynamics in quantum integrable antiferromagnets*,
840 Phys. Rev. B **93**, 174426 (2016), doi:10.1103/PhysRevB.93.174426.
- 841 [58] J. Perk and H. Capel, *Time-dependent xx -correlation functions in the one-dimensional*
842 *XY-model*, Physica A **89**, 265 (1977), doi:10.1016/0378-4371(77)90105-4.
- 843 [59] J. Perk, H. Capel and T. Siskens, *Time correlation functions and ergodic properties in*
844 *the alternating XY-chain*, Physica A **89**, 304 (1977), doi:10.1016/0378-4371(77)90106-
845 6.
- 846 [60] I. Peschel and K. Schotte, *Time correlations in quantum spin chains and the X-ray*
847 *absorption problem*, Z. Phys. B **54**, 305 (1984), doi:10.1007/BF01485827.
- 848 [61] L. Turban, *Exactly solvable spin-1/2 quantum chains with multispin interactions*,
849 Phys. Lett. A **104**, 435 (1984), doi:10.1016/0375-9601(84)90751-5.
- 850 [62] V. Eisler, D. Karevski, T. Platini and I. Peschel, *Entanglement evolution af-*
851 *ter connecting finite to infinite quantum chains*, J. Stat. Mech. P01023 (2008),
852 doi:10.1088/1742-5468/2008/01/p01023.